

Shape, size and robustness: feasible regions in the parameter space of biochemical networks

Madalena Chaves*, Eduardo D. Sontag[†] and Anirvan M. Sengupta[‡]

Abstract

The concept of robustness of regulatory networks has been closely related to the nature of the interactions among genes, and the capability of pattern maintenance or reproducibility. Defining this robustness property is a challenging task, but mathematical models have often associated it to the volume of the space of admissible parameters. Not only the volume of the space but also its topology and geometry contain information on essential aspects of the network, including feasible pathways, switching between two parallel pathways or distinct/disconnected active regions of parameters. A general method is presented here to characterize the space of admissible parameters, by writing it as a semi-algebraic set, and then theoretically analyzing its topology and geometry, as well as volume. This method provides a more objective and complete measure of the robustness of a developmental module. As an illustration, the segment polarity gene network is analyzed.

1 Introduction

For biological networks, the concept of robustness often expresses the idea that the system's regulatory functions should operate correctly under a variety of situations. The network should respond appropriately to various stimuli and recognize meaningful ones (either harmful or favorable), but it should also ignore small (not meaningful) variations in the environment as well as inescapable fluctuations in the abundances of biomolecules involved in the network [1, 2, 3]. One might even speculate that if the networks malfunction easily as a result of mutations then it has low chance of being selected by evolution. In that case one might expect a certain degree of mutational robustness [3, 4].

While it is difficult to define this robustness property in a precise form, it has been associated to the space of admissible kinetic parameters, its volume [3], and the effect of parameter perturbations on the qualitative behavior of the system [1, 2]. Some methods for parameter sensitivity have been developed [5, 6], based essentially on derivatives of variables or fluxes with respect to the system's parameters. The volume of the parameter space can be used as an indication of "how many" parameter combinations are possible, and these are related to the ability of the network to work under a variety of situations. For instance, parameters may range through different orders of magnitude, representing very different environments. However, size is often not a reliable measure for robustness; other quantities, such as shape, play a much more important role, as illustrated in Fig. 1. Analysis of the shape or geometry of the admissible parameter set gives an indication not only of its size, but also how far perturbations around each parameter disrupt the network. A robust biological network will admit small fluctuations in its parameters without changing its qualitative behavior. So, a robust network will be associated to a system whose parameter set has few "narrow pieces"

*Project COMORE, INRIA Sophia Antipolis, 2004 Route des Lucioles - BP 93 06902 Sophia Antipolis, France, mchaves@sophia.inria.fr

[†]BioMaPS Institute for Quantitative Biology and Dep. of Mathematics, Rutgers University, Piscataway, NJ 08854 USA, sontag@math.rutgers.edu

[‡]BioMaPS Institute for Quantitative Biology and Dep. of Physics, Rutgers University, Piscataway, NJ 08854 USA, anirvans@physics.rutgers.edu

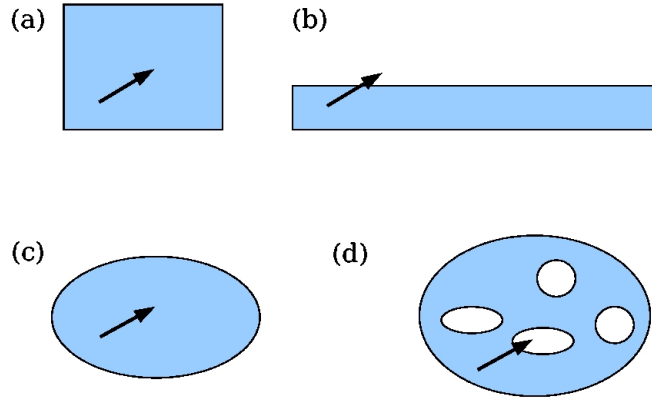


Figure 1: The role of geometry and topology in robustness. Regions (a) and (b) have the same volume, but (b) is less robust: the same perturbation leads out of the space. Regions (c) and (d) also have the same volume, but (d) is not a simply connected set, hence less robust.

and “sharp corners”. In such sets, reasonable parameter fluctuations may occur without leaving the set, hence maintaining the network’s qualitative behavior (compare Fig. 1 (a) and (b)). We can formalize a measure of robustness that is related to having low rate of exit from the region under random walk [4]. The rate of first exit is intrinsically connected to the geometry of the region and is particularly sensitive to narrow directions and not just the overall volume.

To illustrate the importance of parameter space geometry, and the insight it brings to understanding the network, the model of the segment polarity network developed by von Dassow and collaborators [3] will be analyzed. The segment polarity network is part of a cascade of gene families responsible for generating the segmentation of the fruit fly embryo [7]. Genes in earlier stages are transiently expressed, but the segment polarity genes maintain a stable pattern for about three hours. It has been suggested that the segment polarity genes constitute a robust developmental module, capable of autonomously reproducing the same behavior or generating the same gene expression pattern, in response to transient inputs [3, 8, 9]. This robustness would be due to the nature of interactions among genes, rather than the kinetic parameters of the reactions. The model [3] describes the interactions among the principal segment polarity genes, is continuous, and involves cell-to-cell communications and around 50 parameters which are essentially unknown. The authors of [3] explored the model by randomly choosing 240,000 parameter sets out of which about 1,192 (or 0.5%) sets were consistent with the generation (at steady state) of the wild type pattern. To explore the robustness of the network as a property of its interactions, Albert and Othmer [9] developed a Boolean model of the segment polarity network, a discrete logical model where each species has only two states (0 or 1; “OFF” or “ON”), but no kinetic parameters need to be defined. This Boolean model is amenable to various methods for systematic robustness analysis [10, 11, 12]. Ingolia [8] focused on the properties of the (slightly changed) model [3] in individual cells, such as bistability, and extrapolated necessary conditions on parameters to the full intercellular model.

We propose a different approach, that retains the information contained on the kinetic parameters but reduces the model to a logical form with various possible ON levels and species-dependent activation parameters. The admissible set of parameters of the model [3] is analyzed by constructing a cylindrical algebraic decomposition. Among other conclusions, our analysis completely explains the two “missing links” in von Dassow et. al. original model, namely: why the segment polarity pattern can not be recovered without the negative regulation of *engrailed* by Cubitus repressor protein, and why the autocatalytic *wingless* activation pathway vastly increases the network robustness. The present approach shows that, in contrast to volume only estimates, the topology and geometry of this set provide reliable quantitative measures of robustness of a system.

2 Steady states define the feasible parameter space

Previous studies [3, 8] have tested the parameter space by randomly choosing sets of parameters and simulating the continuous model. If the corresponding trajectory reaches a steady state, and if this steady state is compatible with the experimentally observed wild type gene pattern, then the given set of parameters is said to be a “solution” to the modeling problem.

A more efficient and complete study of the parameter space can be devised, by first solving the algebraic equations of the model at steady state, and writing the steady state solutions as a function of the parameters. On the other hand, the steady state solutions are known – the set of elements representing the wild type pattern is denoted by \mathcal{W} – so, one can then look for parameters that yield this pattern. Since many sets of parameters may be expected to yield the wild type pattern, this procedure provides a family of conditions defining regions of “good” or feasible parameters “ p ” for wild-type steady states $x \in \mathcal{W}$.

The von Dassow et. al. model Before proceeding, recall that the model (Appendix B) describes the concentrations of various mRNAs and proteins in a four cell parasegment of the fly embryo, subject to periodic boundary conditions (see also Fig. 2). Here, each cell is assumed to have a square shape, with four faces (see Appendix E). We next very briefly recall the species involved. There are nine species with homogeneous concentration throughout each cell: engrailed mRNA and protein (en and EN), wingless mRNA and (internal) protein (wg and IWG), patched mRNA (ptc), cubitus mRNA, active and repressor proteins (ci , CI, and CN), and hedgehog mRNA (hh). Each of these species has a distinct concentration in each cell (X_i , $i = 1, \dots, 4$). In addition, there are three other species whose concentration varies in each of the four cell faces: external wingless protein (EWG), patched protein (PTC) and hedgehog protein (HH). For each of these species, the concentration in cell i at face j is denoted $X_{i,j}$, $i = 1, \dots, 4$, $j = 1, \dots, 4$. Thus, overall there are: $n = 9 \times 4 + 3 \times 4 \times 4 = 84$ variables. Throughout the paper, the following notation will be used (prime denotes transpose):

$$X = (X_1, X_2, X_3, X_4)', \text{ for } X \in \{en, EN, wg, IWG, ptc, ci, CI, CN, hh\}.$$

and

$$X = (X_{1,1}, X_{1,2}, X_{1,3}, X_{1,4}, X_{2,1}, \dots, X_{4,4})', \text{ for } X \in \{EWG, PTC, HH\}.$$

The total vector of concentrations is:

$$x = (en', EN', wg', IWG', EWG', ptc', PTC', ci', CI', CN', hh', HH').$$

Set of feasible parameters In general, the problem can be formulated mathematically by writing a set of equations dependent on the vector of species concentrations ($x \in \mathbb{R}_{\geq 0}^n$) and the parameter vector ($p \in \mathbb{R}_{> 0}^r$), together with a set of outputs ($y \in \mathbb{R}_{\geq 0}^m$, the available gene expression levels). Introduce functions $f : \mathbb{R}_{\geq 0}^n \times \mathbb{R}_{> 0}^r \rightarrow \mathbb{R}^n$ and $h : \mathbb{R}_{\geq 0}^n \rightarrow \mathcal{Y} \subset \mathbb{R}_{\geq 0}^m$, where $\mathbb{R}_{\geq 0} = \{x \in \mathbb{R} : x_i \geq 0, \text{ for all } i\}$, and consider the system with outputs

$$\frac{dx}{dt} = f(x, p) \tag{1}$$

$$y = h(x) \tag{2}$$

where the function $h(x)$ could be, for instance, a vector listing the concentration of *wingless*, *engrailed*, *hedgehog* and *cubitus*, four of the segment polarity mRNAs which have been experimentally measured. Or, in other words, y is “the phenotype corresponding to the genotype x ”. The wild-type gene expression output set can be defined as:

$$\mathcal{Y}^{\text{WT}} = \{y \in \mathcal{Y} : y = h(x), x \in \mathcal{W}\}.$$

The problem of characterizing the sets of feasible parameters is then reduced to finding all possible parameter vectors p which lead the system to have an output in \mathcal{Y}^{WT} , at steady state. This will be the set of “good” parameters:

$$G = \{ p \in \mathbb{R}_{\geq 0}^r : \exists x \text{ s.t. } f(x, p) = 0 \text{ and } h(x) \in \mathcal{Y}^{\text{WT}} \}. \quad (3)$$

Large Hill coefficients A straightforward approach would be to solve the original system at steady state, obtain expressions for $x \in \mathcal{W}$ in terms of p , and compare these expressions to the outputs in \mathcal{Y}^{WT} :

$$f(x, p) = 0 \Leftrightarrow x = F(p) \quad \text{and} \quad F(p) \in \mathcal{W} \Leftrightarrow p \in G.$$

A possible drawback of this method is that explicit solutions $x = F(p)$ for the original system and then explicit formulas for G may not be easy to compute. On the other hand, many of the equations in the model [3] involve terms of the form (see also Appendix B):

$$\phi(X, \kappa, \nu) = \frac{X^\nu}{\kappa^\nu + X^\nu},$$

meaning that the function ϕ is active (ON), if species X is above a certain threshold κ . The exponent ν , also known as the Hill coefficient, characterizes the steepness of an OFF/ON transition. For large enough exponents, this saturation function becomes very steep, and ϕ becomes practically insensitive to the actual value of ν . As found in [13], coefficients ν must indeed be quite large for the network to achieve robustness: namely in the interval [5.0, 10.0]. This is also the basis of the typical on/off logical interpretation of gene expression. Any such term $\phi(X, \kappa, \nu)$, for large ν , may thus be replaced by a step function with two levels (0 or 1):

$$\theta(X - \kappa) = \begin{cases} 0, & X < \kappa \\ 1, & X > \kappa. \end{cases}$$

Thus, when ν is large:

$$\lim_{\nu \rightarrow \infty} \phi(X, \kappa, \nu) = \theta(X - \kappa), \quad \lim_{\nu \rightarrow \infty} \psi(X, \kappa, \nu) = 1 - \theta(X - \kappa) = \theta(\kappa - X). \quad (4)$$

A composite function of ϕ and ψ also frequently appears in the continuous equations (Appendix B):

$$\phi(X_a \psi(X_b \kappa_b, \nu_b), \kappa_a, \nu_a).$$

This function can be simplified in terms of step functions to:

$$\theta(X_a \theta(\kappa_b - X_b) - \kappa_a) = \theta(X_a - \kappa_a) \theta(\kappa_b - X_b)$$

since

$$\begin{aligned} X_b > \kappa_b &\Rightarrow \theta(\kappa_b - X_b) = 0 \Rightarrow \theta(X_a \theta(\kappa_b - X_b) - \kappa_a) = \theta(-\kappa_a) = 0, \\ X_b < \kappa_b &\Rightarrow \theta(\kappa_b - X_b) = 1 \Rightarrow \theta(X_a \theta(\kappa_b - X_b) - \kappa_a) = \theta(X_a - \kappa_a). \end{aligned}$$

As an example, consider the equation governing *engrailed* from the original model which can be found in [3, 13] (or in Appendix B). In this model the concentration of *engrailed* in cell i (en_i), is positively regulated by external Wingless protein (EWG_i) and negatively regulated by Cubitus repressor protein (CN_i) concentrations (further notation is found in Appendix A):

$$\frac{den_i}{dt} = \frac{1}{H_{en}} \left(\phi(\text{EWG}_i \psi(\text{CN}_i, \kappa_{\text{CN}_i}, \nu_{\text{CN}_i}), \kappa_{\text{WGen}}, \nu_{\text{WGen}}) - en_i \right).$$

For large exponents ν , this simplifies to the equation:

$$\frac{den_i}{dt} = \frac{1}{H_{en}} (\theta(\text{EWG}_{\underline{i}} - \kappa_{wGen})\theta(\kappa_{CNen} - \text{CN}_i) - en_i).$$

To analytically study the space of feasible parameters for the segment polarity network model [3], we will thus consider that all exponents ν are large, and apply method (4) to simplify the original system of equations. The von Dassow et. al. model is then characterized by equations (31)-(42) (Appendix C). The parameters are as in [3], except T_i and U_i , which represent the maximal values of *ptc* and *ci* (respectively), in each cell. These take values in the interval $[0, 1]$ and generalize the possible ON values of *ptc* and *ci* (to be discussed later). In addition, as discussed, the system is assumed to be at steady state, in which case the gene expression pattern must satisfy:

$$en_i = \theta(\text{EWG}_{\underline{i}} - \kappa_{wGen})\theta(\kappa_{CNen} - \text{CN}_i).$$

Applying (4) and then solving the system at steady state yields the set of algebraic equations (43)-(54), which characterize the gene expression pattern of the segment polarity network according to the von Dassow et. al. model.

Maximal (ON) expression levels While some of the species have a normalized maximal expression level (to 1), such as *en* or *hh*, other species may be more generally allowed to have any positive value (namely, *ptc* and *ci*). These maximal expression levels are also treated as parameters. When using (4) to simplify the *patched* equation (24) to (36), we have generalized the equation and added distinct maximal levels of expression in each cell, given by T_i ($i = 1, \dots, 4$). This allows a more accurate representation of experimental data, which shows that *patched* is strongly expressed in every second and fourth cells, weakly expressed in every first cell, and not expressed in every third cell (see [3] for more discussion). Thus we will consider $T_1 < T_2 = T_4$:

$$ptc_{1,2,3,4}^{\text{WT}} = (T_1, T_2, 0, T_2)'. \quad (5)$$

A similar generalization was made to deal with the activation of *cubitus interruptus*. In von Dassow et. al. model, this is due to some external parameters B_i (not governed by a dynamical equation), with a corresponding activity threshold κ_{Bci} . However, for more generality, and to allow distinct maximal levels of expression in each cell, we have replaced each of the terms $\theta(B_i - \kappa_{Bci})$ in (38) by a parameter U_i , $i = 1, \dots, 4$ (50). Furthermore, in characterizing the set of feasible parameters, it will become clear that allowing distinct U_i enlarges the space of possible parameters, by introducing the four regions $G_{C,I}$ to $G_{C,IV}$. Thus the steady state values for the cubitus mRNA are:

$$ci_{1,2,3,4}^{\text{WT}} = (U_1, U_2, 0, U_4)'. \quad (6)$$

Asymmetry in *cubitus* expression (i.e., distinct values U_i) could be due, for instance, to some of the pair rule genes. Sloppy paired, or a combination of Runt and Factor X, regulate the transition from pair rule to segment polarity genes expression, and induce asymmetric anterior/posterior parasegment expression [14].

Finally, note that the maximal expression levels of *wg* are expressed in terms of the parameters α_{Clwg} and α_{wGwg} . From equation (45), there are three possible combinations of the step functions, each leading to a different value for wg_2 . These three possibilities are:

$$w_{Cl} = \frac{\alpha_{Clwg}}{1 + \alpha_{Clwg}}, \quad w_{Cl,WG} = \frac{\alpha_{Clwg} + \alpha_{wGwg}}{1 + \alpha_{Clwg} + \alpha_{wGwg}}, \quad w_{wG} = \frac{\alpha_{wGwg}}{1 + \alpha_{wGwg}},$$

and each reflects a different pathway for *wingless* activation. Indeed, *wingless* can be activated by Cubitus only (in which case the maximal amplitude is given by w_{Cl}), by both Cubitus and Wingless ($w_{Cl,WG}$), or by Wingless only (w_{wG}).

Outputs The next question concerns the choice of an appropriate output function. The gene expression patterns for *engrailed*, *wingless*, *hedgehog*, *cubitus*, and *patched* are among the most well documented, so we will consider the output function $h : \mathbb{R}_{\geq 0}^n \rightarrow \mathbb{R}_{\geq 0}^{20}$:

$$y = h(x) = \begin{pmatrix} h_{en}(x) \\ h_{wg}(x) \\ h_{ptc}(x) \\ h_{ci}(x) \\ h_{hh}(x) \end{pmatrix}. \quad (7)$$

At steady state, both *en* and *hh* are expressed in every third cell [15], which translates into

$$h_{en}(x) = (0, 0, 1, 0)', \quad h_{hh}(x) = (0, 0, 1, 0)', \quad \text{for } x \in \mathcal{W}. \quad (8)$$

Further experimental observations show that *cubitus* is expressed in all but the third cell [16], and *patched* is strongly expressed in every second and fourth [15], but more weakly expressed in every first cell. So:

$$h_{ci}(x) = (U_1, U_2, 0, U_4)', \quad h_{ptc}(x) = (T_1, T_2, 0, T_2)', \quad \text{for } x \in \mathcal{W}. \quad (9)$$

Finally, *wingless* (*wg*) is only expressed in every second cell [15], to the left of *en*, that is:

$$h_{wg}(x) = (0, w, 0, 0)', \quad \text{for } x \in \mathcal{W}. \quad (10)$$

To summarize, in this example, the set of output values at steady state is:

$$\mathcal{Y}^{\text{WT}} = \{((0, 0, 1, 0), (0, w, 0, 0), (T_1, T_2, 0, T_2), (U_1, U_2, 0, U_4), (0, 0, 1, 0))' : w, T_1, T_2, U_1, U_2, U_4 > 0, T_1 < T_2\}. \quad (11)$$

The first result to be noted is that there is a *unique* steady state $x = x(p) \in \mathcal{W}$ for each set of parameters p :

Theorem 1. *Let f be the function $\mathbb{R}_{\geq 0}^n \times \mathbb{R}_{\geq 0}^r \rightarrow \mathbb{R}^n$ given by (31)-(42), and h be the function $\mathbb{R}_{\geq 0}^n \rightarrow \mathcal{Y}$ given by (7). Define G as in (3). Then, there exists a function $F : G \rightarrow \mathbb{R}_{\geq 0}^n$ such that, for each $p \in \mathbb{R}_{\geq 0}^r$ and each $x \in \mathbb{R}_{\geq 0}^n$,*

$$f(x, p) = 0 \text{ and } h(x) \in \mathcal{Y}^{\text{WT}} \text{ imply } x = F(p).$$

Proof. Pick any $p \in G$, and an $x \in \mathbb{R}_{\geq 0}^n$ satisfying $f(x, p) = 0$ and $h(x) \in \mathcal{Y}^{\text{WT}}$. The equations $f(x, p) = 0$ can be simplified to yield (43)-(54). We must check that these equations are all consistent and admit only one solution. Since all mRNAs *en*, *wg*, *ptc*, *ci*, and *hh* are provided by $h(x)$, we must solve for the proteins, and then substitute these back into the equations for the mRNAs, to check consistency.

The Engrailed protein is straightforward: $\text{EN} = en$. We start by solving for EWG, with $wg = (0, w, 0, 0)'$ as given. First note that the matrix M is diagonally dominant, by adding up the entries in any column:

$$- (H_{\text{IWG}}^{-1} + r_{\text{endo}} + r_M + 2r_{LM}) + 2r_{LM} + r_M + 4h = -H_{\text{IWG}}^{-1} - r_{\text{endo}} \frac{1}{1 + H_{\text{IWG}} r_{\text{exo}}} \quad (12)$$

which is always a negative quantity. By Geršgorin's Theorem, all eigenvalues of M are contained in the disk centered at $-d + h$ with radius $2r_{LM} + r_M + 3h$, therefore all eigenvalues have negative real parts. Thus, the matrix M is symmetric and negative definite, and since the right-hand-side vector in (47) is also non-positive, there is a unique solution

$$\text{EWG} = -\frac{1}{4} \frac{r_{\text{exo}}}{1 + H_{\text{IWG}} r_{\text{exo}}} M^{-1} \widetilde{wg}$$

which is real and positive, *for each set of parameters* p . Once we have EWG, we can immediately solve for IWG from (46).

The solution for PTC and HH can also be exactly and uniquely computed from (49) and (54), for any output $ptc = (T_1, T_2, 0, T_2)'$ (this calculation is shown Appendix F).

Finally, one can now straightforwardly and uniquely compute the values of CI and CN, from (51) and (52), and the values of ci and PTC.

The last step is the substitution of EN, EWG, IWG, PTC, HH, CI and CN back into the equations for the mRNAs (43), (45), (48), (50), and (53). But, since $p \in G$, by definition we are guaranteed that these equalities are indeed satisfied. ■

Missing link: *engrailed* regulation by Cubitus repressor A second result from our model formulation is the explanation of a “missing link” in a first version of the model proposed by von Dassow et. al. [3]. In this first version, *engrailed* was regulated only by EWG, and no feasible parameter sets were found. Indeed, below (Theorem 2) we prove that, *for any set of parameters*, the mechanism for *wingless* regulation generates a strong symmetry in the steady state expression of external Wingless. This symmetry effectively prevents any asymmetry arising in *en* due to EWG only.

Theorem 2. *Let $w > 0$ and assume $wg^{WT} = (0, w, 0, 0)'$. Then, at steady state:*

$$EWG_4^{WT} < EWG_1^{WT} = EWG_3^{WT} < EWG_2^{WT}. \quad (13)$$

The proof is based on a sequence of algebraic calculations, and is shown in Appendix E. Now, consider the steady state equation for *engrailed*, when no dependence on CN is assumed:

$$en_i^{WT} = \theta(EWG_i^{WT} - \kappa_{WGen})$$

Compare to the output (8):

$$h_{en}(x) = (0, 0, 1, 0)'$$

Then, from the definition of θ , for consistency in our model it is necessary that:

$$\begin{aligned} EWG_i^{WT} &< \kappa_{WGen}, \quad \text{for } i = 1, 2, 4 \\ EWG_3^{WT} &> \kappa_{WGen}. \end{aligned}$$

However, by (13), the inequalities for $i = 1, 2$ and $i = 3$ are incompatible. This means that, due to the symmetry in Wingless distribution, such a simple regulation of *en* can never lead to the segment polarity pattern. Thus *engrailed* requires regulation by some other factor, in this case repression by the Cubitus protein (CN), as in (43). In order to obtain repression of *en* in the first and second cells, one can now ask:

$$\begin{aligned} CN_1^{WT} &> \kappa_{CNen}, \quad CN_2^{WT} > \kappa_{CNen} \\ EWG_3^{WT} &> \kappa_{WGen} \quad \text{and} \quad CN_3^{WT} < \kappa_{CNen} \\ EWG_4^{WT} &< \kappa_{WGen} \quad \text{or} \quad CN_4^{WT} > \kappa_{CNen} \end{aligned}$$

that is, CN is responsible for repression in both the first and second cells. This means that, at steady state, CN must be expressed in both the first and second cells. This in turn requires the presence of Patched protein in both the first and second cells. On the other hand, from Appendix F, we know that a steady state $x \in \mathcal{W}$ with $h(x) \in \mathcal{Y}^{WT}$, implies $ptc_1^{WT} = PTC_1^{WT}$, and also $PTC_2^{WT} = PTC_4^{WT}$. This can be stated as:

Lemma 2.1. Consider system (1) and assume that, at steady state, the output set is \mathcal{Y}^{WT} . Then $ptc_1^{WT} = PTC_1^{WT} \neq 0$. If $ptc^{WT} = (T_1, T_2, 0, T_2)'$ with $T_1 < T_2$, then $PTC_1^{WT} = T_1$ and $PTC_2^{WT} = PTC_4^{WT} > 0$. ■

While *patched* expression is typically weaker in the first than in second and fourth cells (see [3]), this shows that it is nevertheless necessary, that is, the segment polarity gene pattern obtains only when $T_1 > 0$. The discussion on CN leads to the following conclusion:

Lemma 2.2. Consider system (1) and assume that, at steady state, the output set is \mathcal{Y}^{WT} . Let $ptc^{\text{WT}} = (T_1, T_2, 0, T_2)'$ with $T_1 < T_2$. Then $\text{PTC}_{1,2}^{\text{WT}} > \kappa_{\text{PTCCI}}$ and

$$\text{CI}_i^{\text{WT}} = U_i \frac{1}{1 + H_{\text{CI}} C_{\text{CI}}}, \quad \text{CN}_i^{\text{WT}} = U_i \frac{H_{\text{CI}} C_{\text{CI}}}{1 + H_{\text{CI}} C_{\text{CI}}}, \quad i = 1, 2, 4, \quad (14)$$

and $\text{CI}_3^{\text{WT}} = \text{CN}_3^{\text{WT}} = ci_3^{\text{WT}} = 0$.

Proof. Theorem 2 and the subsequent discussion shows that $\text{CN}_{1,2}^{\text{WT}} \neq 0$ is needed. From (52), this can only be achieved by asking $\text{PTC}_{1,2}^{\text{WT}} > \kappa_{\text{PTCCI}}$. By Lemma 2.1, it also holds that $\text{PTC}_2^{\text{WT}} = \text{PTC}_4^{\text{WT}} > \kappa_{\text{PTCCI}}$. This means that both (51) and (52) can be simplified to (14), at steady state. On the third cell, $\text{CI}_3^{\text{WT}} = \text{CN}_3^{\text{WT}} = 0$ because the output is zero. ■

3 A cylindrical algebraic decomposition of the parameter space

The algebraic equations $f(x, p) = 0$ together with $h(x) \in \mathcal{Y}^{\text{WT}}$ are a representation of the set of good parameters G , though not providing as yet explicit conditions on p . An explicit characterization of the parameters p may be obtained by calculating a cylindrical algebraic decomposition (CAD) of G : this is a special type of representation of G as a finite union of disjoint connected components. A CAD will provide a hierarchy of inequalities on p_1, p_2, \dots, p_r , from which the volume of G , as well as its geometry and topology, may be deduced.

Computing the cylindrical algebraic decomposition of a semi-algebraic set is a complex problem, but various standard algorithms are available [17, 18]. Several software packages have been developed, for instance QEPAD [19], (based in [20]) and in Mathematica [21]. See also [22] for an overview of available software, current applications, and many other related references. Common applications of CADs include computation of the controllable or reachable sets in hybrid systems [23]. Constructing a CAD involves the use of symbolic computation and, while various improvements have been achieved, it still is a time-consuming problem. For instance, the estimated maximum time for the algorithm [17] is dominated by “ $2^{2^k N}$ ”, where N is the length of the input formula and $0 < k \leq 8$. Fortunately, in view of these computational complexity difficulties, in the present example it is relatively easy to directly compute a CAD without using general methods, and we will do so.

For equations (43)-(54), subject to (8)-(10), a cylindrical algebraic decomposition can be constructed in which several parameters (Table 6) are free to take any values (within physiological restrictions only). At the next level, parameters in Table 7 have constraints which depend only on those parameters given in Table 6. The last level is formed by the parameters in Table 8, whose constraints depend on parameters from both previous levels (Tables 6 and 7), thus defining a polyhedron.

Following the model of von Dassow et. al., there are two possible parallel pathways for *wingless* activation: either by the Cubitus interruptus protein (CI), or through auto-activation; both pathways could be simultaneously activating *wingless* production. Since the activation constants α_{CIwg} and α_{WGwg} , are free parameters, in each of the three cases wg_2^{WT} will have a different ON level (respectively, w_{CI} , w_{WG} , or $w_{\text{CI,WG}}$). Computation of EWG and IWG depends on wg_2^{WT} , so each of these three cases must be separately analyzed for feasibility. For both pathways, exact analytic computation of $\text{PTC}_{i,j}$ and $\text{HH}_{i,j}$ ($i, j = 1, \dots, 4$) is also carried out (see Appendix F). Several disconnected regions of parameters will be defined by the levels of *cubitus*, $U_{1,2,4}$.

Five disconnected regions When only CI and CN regulate *wingless* expression, it is easy to see from (45), (10) and (14) that:

$$\left(U_i \frac{1}{1 + H_{\text{CI}} C_{\text{CI}}} < \kappa_{\text{Clwg}} \quad \text{or} \quad U_i \frac{H_{\text{CI}} C_{\text{CI}}}{1 + H_{\text{CI}} C_{\text{CI}}} > \kappa_{\text{CNwg}} \right) \quad \text{and} \quad \text{IWG}_i < \kappa_{\text{WGwg}} \quad (15)$$

for $i = 1, 3, 4$, and

$$U_2 \frac{1}{1 + H_{\text{CI}} C_{\text{CI}}} > \kappa_{\text{Clwg}} \quad \text{and} \quad U_2 \frac{H_{\text{CI}} C_{\text{CI}}}{1 + H_{\text{CI}} C_{\text{CI}}} < \kappa_{\text{CNwg}} \quad \text{and} \quad \text{IWG}_2 < \kappa_{\text{WGwg}}. \quad (16)$$

From observation of (15), (16) it is clear that the situations $U_2 = U_1$ or $U_2 = U_4$ are not well defined, since contradictory constraints are imposed on κ_{Clwg} and κ_{CNwg} . So, the regions of parameters satisfying $U_2 = U_1$ or $U_2 = U_4$ are not feasible. This divides the set G into at least four disconnected components, divided by the hyperplanes $U_2 = U_1$ or $U_2 = U_4$ ($G_{\text{C,I}}$, $G_{\text{C,II}}$, $G_{\text{C,III}}$, and $G_{\text{C,IV}}$ in Fig. 3). A similar argument holds for the case when both pathways contribute to activation of *wingless* on the second cell. The four disconnected regions of parameters are identified in Table 8.

Finally, the third case (auto-activation pathway only), introduces a fifth component of G (G_{Auto}), which must be disconnected from either of the previous four components. This is clear, by contrasting the necessary conditions in the second cell for either case (compare to (16)):

$$\left(U_2 \frac{1}{1 + H_{\text{CI}} C_{\text{CI}}} < \kappa_{\text{Clwg}} \quad \text{or} \quad U_2 \frac{H_{\text{CI}} C_{\text{CI}}}{1 + H_{\text{CI}} C_{\text{CI}}} > \kappa_{\text{CNwg}} \right) \quad \text{and} \quad \text{IWG}_2 > \kappa_{\text{WGwg}}. \quad (17)$$

The five disconnected components are thus first defined by U_1 , U_2 , and U_4 , and then by κ_{Clwg} and κ_{CNwg} . The projection on the $(\kappa_{\text{Clwg}}, \kappa_{\text{CNwg}}, \kappa_{\text{WGwg}})$ -dimensions compares two of these components ($G_{\text{C,II}}$ and G_{Auto}), both polyhedrons (Fig. 4).

The cylindrical algebraic decomposition is shown in detail in Appendix G, and summarized in Tables 6,7,8. Each of the five components, $G_\gamma \in \{G_{\text{C,I}}, G_{\text{C,II}}, G_{\text{C,III}}, G_{\text{C,IV}}, G_{\text{Auto}}\}$ is thus described by a hierarchy of sets of the form:

$$\begin{aligned} S_{1,\gamma} &= (a_\gamma, b_\gamma) \subset \mathbb{R} \\ S_{i,\gamma} &= \{(x, x_i) \in \mathbb{R}^i : x \in S_{i-1,\gamma}, \alpha_{i,\gamma}(x) < x_i < \beta_{i,\gamma}(x)\} \subset \mathbb{R}^i \end{aligned} \quad (18)$$

for $i = 2, \dots, N$, where $\alpha_{i,\gamma}, \beta_{i,\gamma} : S_{i-1,\gamma} \rightarrow \mathbb{R}_{>0}$ and $S_{N,\gamma} = G_\gamma$. It can be shown that each G_γ is in fact topologically equivalent to the unitary open hypercube, and hence topologically trivial.

Theorem 3. *For each G_γ , the set $S_N = S_{N,\gamma}$, as obtained from (18), is homeomorphic to $(0, 1)^N$.*

Proof. Pick any G_γ , and drop the subscript γ , for simplicity of notation. To argue by induction, note that the set S_1 is clearly homeomorphic to $(0, 1)$. For $i \geq 2$, assume that S_{i-1} is homeomorphic to $(0, 1)^{i-1}$. Next, define the following continuous function:

$$\varphi_i : S_{i-1} \times (0, 1) \rightarrow S_{i-1} \times \mathbb{R}, \quad \varphi_i(x, t) = (x, f_i(x) + t(g_i(x) - f_i(x))).$$

For each fixed x , $\alpha_i(x) < \alpha_i(x) + t(\beta_i(x) - \alpha_i(x)) < \beta_i(x)$ for all $t \in (0, 1)$. Therefore, φ_i maps into S_i . On the other hand, φ_i has an inverse function defined on S_i and continuous, given by:

$$\varphi_i^{-1} : S_i \rightarrow S_{i-1} \times (0, 1), \quad \varphi_i^{-1}(x, y) = \left(x, \frac{y - \alpha_i(x)}{\beta_i(x) - \alpha_i(x)} \right).$$

So S_i is homeomorphic to $S_{i-1} \times (0, 1)$, and therefore, by inductive hypothesis, to $(0, 1)^i$, as we wanted to show. ■

Relative volume and the second missing link Once the parameter set G is characterized by writing intervals for the various parameters in the form (18), it is very easy to compute the (relative) volumes of the disconnected components. Note that in each component only the intervals for U_1, U_2, U_4 , and $\kappa_{CNen}, \kappa_{WGen}, \kappa_{Clwg}, \kappa_{CNwg}, \kappa_{WGwg}$ vary; constraints on the remaining parameters are common to all components. Following a Monte Carlo approach, the parameters in Tables 6,7 are chosen first, and then $\kappa_{Clwg}, \kappa_{CNwg}, \kappa_{WGwg}$ from the unitary cube (all parameters are randomly chosen from uniform distributions in the given intervals). It is next checked whether the parameter set falls in any of the components $G_{C,I}, G_{C,II}, G_{C,III}, G_{C,IV}, G_{Auto}$, or outside G . This method provides an estimate of the volumes of each disconnected component, when projected into the $(\kappa_{CNen}, \kappa_{WGen}, \kappa_{Clwg}, \kappa_{CNwg}, \kappa_{WGwg})$ dimensions, as the fraction of parameter sets that fall into each component. The volume of this 5-dimensional cube occupied by feasible parameter sets is only about 0.7%. As is illustrated by the polyhedrons in Fig. 4, component G_{Auto} is much larger than the others – approximately 40 to 270 times larger.

Table 1: Relative volumes of the five disconnected components. In component G_{Auto} , only auto-activation leads to *wingless* expression. In components $G_{C,I}, G_{C,II}, G_{C,III}$, and $G_{C,IV}$, CI always activates *wingless* expression. Total number of parameter sets generated: 1×10^7 . Number of feasible parameter sets: 70026.

Component	Volume
$G_{C,I}$	1.6×10^{-4}
$G_{C,II}$	0.25×10^{-4}
$G_{C,III}$	0.86×10^{-4}
$G_{C,IV}$	0.46×10^{-4}
G_{Auto}	67×10^{-4}

The large difference observed between $G_{C,I}-G_{C,IV}$ and G_{Auto} explains the second “missing link” in the first version of von Dassow et. al. model, namely the *wingless* autocatalytic activation. Note that the presence of this link greatly increases the total volume of the feasible parameter space: in fact the region G_{Auto} is 95% of the total volume.

Parameter tendencies As described above, the parameter space for the segment polarity network can be described by a CAD, a hierarchy of inequalities on the parameters where an interval is explicitly given for each parameter. At the base of this hierarchy, there is a first group of parameters whose intervals correspond simply to physiological values, as in Table 6. The intervals for the remaining parameters have bounds which depend on the parameters in the first group (Tables 7 and 8). In any case, one may ask how the parameters are distributed in their intervals, whether each parameter p_i is more likely to attain high or low values more frequently, or whether a “tendency” for each parameter p_i be identified. An answer to this question is obtained by randomly generating parameters in the full parameter space G , and computing the distribution of each parameter. Taking all the parameter sets generated to compute the relative volumes of the five disconnected components of G , and computing a histogram for each parameter, the result shown on Fig. 5 is obtained. As expected, many parameters have a uniform distribution, as their values do not influence the final outcome of the network in any particular way (for instance, most half-lives). Other parameters exhibit a marked tendency for higher (e.g., κ_{CNptc}), medium (e.g., κ_{WGwg}) or lower (e.g., κ_{Clptc}) values. All the parameters that exhibit a marked tendency are listed in Table 2, and classified according to their function in the network: for instance, κ_{CNptc} represents the repression of *ptc* by CN, and therefore, high values of κ_{CNptc} correspond to a weak repression.

A very similar analysis was performed by von Dassow and Odell [13], who also plotted the distribution of their family of feasible parameters to determine possible constraints for each parameter. Overall, our results agree very well with those of von Dassow and Odell: most tendencies found by these authors (see

Fig. 6 and Table 1 of [13]) are confirmed by our parameter space analysis. There are only five exceptions, where our analysis showed no tendency (compare columns 3 and 4 of Table 2), suggesting that these five parameters can, in fact, take values in a larger set, implying that the parameter space is larger than estimated in [13]. From these exceptions, κ_{ENci} , κ_{ENhh} , κ_{CNhh} , and r_{endoWG} all belong to the group of parameters which can be freely chosen. The other parameter is κ_{Clwg} , which depends on the disconnected regions, and again our analysis shows that this pair has no preferred tendency.

A more detailed examination of the conditions on κ_{Clwg} and κ_{CNwg} turns out to be very illuminating. First, note that κ_{Clwg} and κ_{CNwg} define the five components, in the sense that distinct intervals for these two parameters are given in each component. Thus, it may be expected that the distribution of these parameters varies in each region (Table 3). Indeed, by plotting the histograms for κ_{Clwg} and κ_{CNwg} for each region alone, we note that these show a marked tendency in components $G_{C,I} - G_{C,IV}$, for low κ_{Clwg} and high κ_{CNwg} . In contrast, the distributions of κ_{Clwg} and κ_{CNwg} for region G_{Auto} alone show an opposite tendency. This is consistent with the fact that the volume of G_{Auto} is about 95% of G and, therefore, it dominates the overall tendency. Note also that, in the four components $G_{C,I} - G_{C,IV}$, it always holds that $\kappa_{Clwg} < \kappa_{CNwg}$, clearly in agreement with the tendency observed for our parameter sets. In component G_{Auto} , the parameters κ_{Clwg} and κ_{CNwg} must satisfy constraints that contradict those of $G_{C,I} - G_{C,IV}$, but not necessarily exactly opposite constraints (see Table 8). Thus more freedom results for the choice of κ_{Clwg} and κ_{CNwg} in G_{Auto} . The tendency of κ_{Clwg} and κ_{CNwg} in $G_{C,I} - G_{C,IV}$ is, however, the opposite of that observed by von Dassow and Odell, a fact that can be explained once again by the “second missing link”. Indeed, since all feasible parameter sets in [3, 13] were found only after adding the autocatalytic *wingless* activation link, it can be inferred that those parameters belong to region G_{Auto} . We conclude that the parameter space is larger than estimated by von Dassow and Odell.

Table 2: Comparison between the constraints identified by von Dassow and Odell [13], and the exact constraints given by the five regions defined above. Total number of parameters generated in G : 70026.

Parameter	Description	Tendency ([13], Table 1)	Tendency (within G)
κ_{WGen}	WG activation of en	Moderate	Moderate
κ_{CNen}	CN repression of en	Strong	Strong
κ_{WGwg}	WG autoactivation	Moderate	Moderate
κ_{Clwg}	CI activation of wg	Weak	—
κ_{CNwg}	CN repression of wg	Strong	Strong
κ_{Clptc}	CI activation of ptc	Strong	Strong
κ_{CNptc}	CN repression of ptc	Weak	Weak
κ_{ENci}	EN repression of ci	Moderate	—
κ_{PTCCI}	PTC stimulation of CI cleavage	Strong	Strong
κ_{ENhh}	EN activation of hh	Weak	—
κ_{CNhh}	CN repression of hh	Strong	—
C_{CI}	Maximal cleavage rate of CI	Rapid	Rapid
H_{IWG}	Half-life of intracellular WG	Short	Short
r_{endoWG}	Rate of WG endocytosis	Slow	—
r_{exoWG}	Rate of WG exocytosis	Moderately slow	Moderately fast
T_{MxferWG}	Rate of WG cell-to-cell exchange	Slow	Slow
α_{WGwg}	Maximal WG autocatalytic rate	—	Moderately rapid

Table 3: Influence of the autocatalytic WG activation link in the parameter distribution.

Parameter	Tendency ([13], Table 1)	Tendency G_{Auto} (WG \rightarrow wg)	Tendency $G_{\text{C,I}}, G_{\text{C,II}}, G_{\text{C,III}}, G_{\text{C,IV}}$ (WG \nrightarrow wg)
κ_{Clwg}	Weak	Weak	Strong
κ_{CNwg}	Strong	(Moderately) Strong	Weak

4 Geometry and robustness

The volume estimates for the parameter space regions give an idea of “how many” parameter combinations are possible. But volume alone is often not a reliable measure for robustness, as illustrated in Fig. 1. The shape or geometry of the parameter space regions also shows how far perturbations around each parameter will disrupt the network. Thus, parameter regions exhibiting “narrow” pieces or “sharp” corners indicate a lower level of robustness in the network. One way to explore the shape of a given multi-dimensional set is to consider a random point (p^0) and follow a random walk in space ($p^k = p^{k-1} + dp^k$, $k = 1, 2, \dots$), where each step has the same absolute length ($|dp^k| = a_0$), but a random direction. Then record the number of steps needed for the point to exit the given set. Repeating this procedure for many points in the set, the probability that a point leaves the set after t steps can be computed.

The random walk could be interpreted as parameter changes due to evolution, and the probability of exiting after t steps represents the probability that the network is no longer capable of correctly performing its function (for instance, when a lethal mutation occurs). Studying the first exit problem is the natural thing to do in certain evolutionary models. Suppose we consider a fitness landscape on the parameter space where the functioning regions have a fixed high fitness and every other region has zero fitness. If we consider a space of alleles to be nearly continuous and model the effect of mutation as diffusion in this space, as is often done in the adaptive dynamics literature [24], we find that we need to compute the mutation load, namely the rate of death from exiting the high fitness region. This idea was previously used in the context of transcriptional networks [4].

To explore the shape of the regions $G_{\text{C,I}}$ to G_{Auto} , Algorithm I uses a random walk in the parameter space, and checks “exit times” as well as the “failed parameters”.

Algorithm I

Pick a positive number a_0 to be the constant magnitude of the random walk step.

Repeat points 1-4 (run q), Q times.

1. Step 0: generate a point $p^0 = (p_1^0, \dots, p_m^0)'$ at random in the parameter region G_γ ;
2. Step $k - 1/2$, $k \geq 1$: generate a random perturbation $dp^k \in [-a_0, a_0]^m$, such that $|dp^k| = a_0$;¹
3. Step k , $k \geq 1$: check if $p^k = p^{k-1} + dp^k$ is still in G_γ ;
4. Check. The random walk exits the parameter region at time t if $p^k \in G_\gamma$ for $k < t$ but $p^t \notin G_\gamma$.
Let $p_{j_1}^t, \dots, p_{j_J}^t$ be parameters that fail to satisfy the hierarchy of conditions which defines G_γ .
Update the exit times vector: $\text{exit}(q) = t$.
Update the failed parameters vector: $\text{failpar}(q) = [j_1, \dots, j_J]$.

¹This step corresponds to generating a random point from a uniform distribution over the hypersphere in n dimensions, which can be achieved by the Box and Muller transformation [25]. Briefly, for $i = 1, \dots, n$ pick z_i randomly from a gaussian distribution of mean zero and variance one. Then normalize to obtain $z = (z_1, \dots, z_n) / \sqrt{z_1^2 + \dots + z_n^2}$.

To interpret the numerical results obtained with Algorithm I, define the probability that a mutation takes place in the first t steps by:

$$P_{\text{mut}}(t) = \frac{1}{Q} \text{card}(I_t), \quad I_t = \{q \in \mathbb{N} : \text{exit}(q) \leq t\},$$

where $\text{card}(\cdot)$ denotes the cardinality of a set. Algorithm I was applied to each component of the feasible parameter space of the segment polarity network, with $a_0 = 1 \times 10^{-3}$ and $Q = 4000$. Two striking facts are revealed. First, with a significant probability, fluctuations in the parameters will drive the system from the operating regions $G_{\text{C,I}}$, $G_{\text{C,II}}$, $G_{\text{C,III}}$, or $G_{\text{C,IV}}$, to the region G_{Auto} and, conversely, switching was also observed from G_{Auto} to the other four (see the switching column in Table 4). Recalling the difference between G_{Auto} and the other four components, this means that, in a significant number cases, the network responds to perturbations by switching to an alternative biological pathway, rather than break down. A second fact is that only a very small number of parameters (six out of 39, namely κ_{CNen} , κ_{WGen} , κ_{Clptc} , κ_{PTCCI} , κ_{Clwg} , κ_{CNwg}) are responsible for above 90% of network failures or mutations. The percentage of cases where each of these parameters failed is shown in Table 4.

Table 4: Fragile parameters.

G_γ	% switching	% failed	% failed	% failed	% failed	% failed	% failed
		κ_{CNen}	κ_{WGen}	κ_{Clptc}	κ_{PTCCI}	κ_{Clwg}	κ_{CNwg}
$G_{\text{C,I}}$	1.21% (to G_{Auto})	5.4%	6.3%	20.0%	4.4	50.8%	5.6%
$G_{\text{C,II}}$	0.88% (to G_{Auto})	4.7%	5.6%	17.2%	4.3	40.0%	18.7%
$G_{\text{C,III}}$	1.50% (to G_{Auto})	6.2%	5.2%	30.8%	4.1	35.0%	11.5%
$G_{\text{C,IV}}$	1.16% (to G_{Auto})	4.9%	5.3%	16.8%	5.0	40.1%	18.9%
G_{Auto}	0.02% (to $G_{\text{C,I}}-G_{\text{C,IV}}$)	8.5%	5.7%	21.2%	4.8	31.4%	18.8%

Calculating the distribution function P_{mut} shows that the probability of mutation increases very rapidly for small times, in all five components (see Fig. 6) – this indicates a low robustness of the network, because it is very likely that a very small number of fluctuations leads out of the feasible parameter space. To compare the results for the five components, we computed some quantities of interest. A possible indicator of robustness is $T_{1/2}$, defined as the time for which there is a 50% chance that the system has already suffered a mutation. Low $T_{1/2}$ indicates a system which has a low robustness to perturbations. Another indicator is $P_{\text{mut}}(10)$, which gives the probability that the system has been disrupted after only 10 perturbation steps. Similarly, the values $P_{\text{mut}}(100)$, $P_{\text{mut}}(1000)$, and $P_{\text{mut}}(10000)$ are also shown for comparison. The computed values are summarized in Table 5. Comparison of the values for $T_{1/2}$ and $P_{\text{mut}}(10^d)$ ($d = 1, \dots, 4$) in the five

Table 5: Indicators of robustness.

G_γ	$T_{1/2}$	$P_{\text{mut}}(10)$	$P_{\text{mut}}(100)$	$P_{\text{mut}}(1000)$	$P_{\text{mut}}(10000)$
$G_{\text{C,I}}$	18	0.40	0.74	0.94	0.99
$G_{\text{C,II}}$	23	0.37	0.72	0.94	0.99
$G_{\text{C,III}}$	19	0.40	0.72	0.93	0.99
$G_{\text{C,IV}}$	23	0.37	0.73	0.94	0.99
G_{Auto}	309	0.30	0.41	0.61	0.88

regions, shows clearly that the components $G_{\text{C,I}}$ to $G_{\text{C,IV}}$ result in a less robust network, while G_{Auto} exhibits a much higher level of robustness. Furthermore, there is a non-negligible probability ($\approx 1\%$) that the network

switches from the other components to G_{Auto} instead of breaking down, thus contributing to the robustness level of this component. Distinguishing the levels of robustness among the four regions $G_{\text{C,I}}$ to $G_{\text{C,IV}}$ is not straightforward, since the indicators $P_{\text{mut}}(10^d)$ and $T_{1/2}$ are very similar.

As noted above, only six out of 39 parameters are responsible for over 90% of failures. Curiously, two of these parameters satisfies constraints which are in fact independent of the regions (κ_{Clptc} and κ_{PTCCl} , see Table 7). So, the numerical results clearly show that the parameter space is very narrow in the directions defined by κ_{Clptc} and κ_{PTCCl} . The other critical directions are defined by κ_{Clwg} and κ_{CNwg} , and κ_{CNen} and κ_{WGen} , which satisfy different conditions in each of the five parameter regions (Table 8). Together with common parameter κ_{Clptc} , the parameters that regulate activation and inhibition of *wingless* by Cubitus proteins (κ_{Clwg} and κ_{CNwg}) are the most critical.

The main conclusion from Algorithm I clearly follows the preliminary estimates of the relative volumes (compare Tables 1 and 5, both concluding that G_{Auto} is more robust than the other four components). But the geometry analysis reveals three new fundamental results: (i) the system increases its robustness to environment perturbations by switching to an alternative biological pathway. The switching event may be from a “small” to a “large” region but also, more remarkably, from a “large” to a “small”; (ii) the lack of robustness is due not only to small sized regions, but in part to critical parameters (κ_{Clptc} and κ_{PTCCl}), which define directions along which the parameter space is globally very narrow; (iii) the volume alone is not a reliable measure of robustness, since volume (Table 1) and the indicator $T_{1/2}$ provide different robustness classifications for components $G_{\text{C,I}}$ to $G_{\text{C,IV}}$. For instance, the volume of $G_{\text{C,II}}$ is apparently the smallest (an indicator of low robustness), but $T_{1/2}$ is the largest (an indicator of high robustness), suggesting that the shape of the region does plays an important role. In contrast, the numbers $P_{\text{mut}}(10^d)$ are very similar, suggesting that robustness levels of $G_{\text{C,I}}$ to $G_{\text{C,IV}}$ are in fact very similar. However, it should be noted that neither volume nor $T_{1/2}$ provide conclusive information on the relative levels of robustness of $G_{\text{C,I}}$ to $G_{\text{C,IV}}$. In particular, note that $T_{1/2}$ depends on the magnitude of the random walk step - other numerical experiments were performed with different a_0 values (not shown), and the comparison results are unchanged.

5 Discussion and conclusions

Analysis of the feasible parameter set, by estimating its volume, identifying connected components, and its geometric properties are valuable tools for establishing and quantifying robustness in regulatory networks. The concept of robustness, in the sense that the system’s regulatory functions should operate correctly under a variety of situations, is closely related to the parameter space and the effect of parameter perturbations. In this context, our analysis suggests that the segment polarity network is vulnerable to perturbations in its parameters. Indeed, the first striking result from our analysis is that the feasible parameter space is composed of five disconnected components. An implication of this topological characterization is a diminished capacity of the network to respond well to environmental perturbations. Random fluctuations will often drive the system to a set of parameters outside any feasible region, and thus lead to a break down of the network or a different phenotype. Indeed, as the results of Algorithm I show, successive random perturbations to the parameters will drive the system out of the feasible parameter set, with a large probability. For instance, if parameters are randomly perturbed for up to 10 times, each of magnitude 1×10^{-3} in any direction, there is a 30% probability that the system will fail to operate correctly (see Table 5, column $P_{\text{mut}}(10)$). On the other hand, it is possible that a series of fluctuations in the environment may drive the system to adopt an alternative biochemical pathway, and thus “jump” from one feasible component to another (with probability 1%, see Table 4).

As the group of most fragile parameters suggest, the Cubitus-*wingless* interactions are at the basis of the appearance of disconnected regions of parameters. Dis-connectivity in the space of parameters can be traced in large part to an incompatibility of Cubitus repression functions in the second cell: CN_2 should be present to repress *engrailed* expression, but should be absent to enhance CI_2 activation of *wingless*. To increase the network’s robustness to environmental fluctuations, the segment polarity model should account

for *engrailed* regulation by other factor than Cubitus. One possibility is to include regulation by pair-rule gene products, such as Sloppy paired, as explored both in [9] and [8]. An external factor, again possibly from the pair-rule genes, will also play a major role in establishing asymmetry in the *cubitus* levels (U_i). These contribute to a larger admissible parameter space, and together with an improved *engrailed* regulation, will greatly enhance robustness of the segment polarity network in maintaining its pattern. An extension of the current analysis including the regulation by Sloppy paired is currently in preparation by A. Dayarian at one of our labs [26].

Both the volume estimates and the probability of failure or mutation (P_{mut}) in each component indicate that G_{Auto} is the most robust parameter region, while $G_{\text{C.I}}$, $G_{\text{C.II}}$, $G_{\text{C.III}}$ and $G_{\text{C.IV}}$ are less robust regions, all at the same level. However, volume is not a reliable indicator of robustness by itself, and fails to predict alternative robustness mechanisms. Additional knowledge on the network mechanisms has been gained with the geometry analysis. A noteworthy fact is the non-negligible probability (1%) that fluctuations in the parameters in regions $G_{\text{C.I}}$ to $G_{\text{C.IV}}$ result in a switch to the region G_{Auto} , and remarkably (but with lower probability 0.02%) also from G_{Auto} to the others. Of the five disconnected components, $G_{\text{C.I}}$, $G_{\text{C.II}}$, $G_{\text{C.III}}$, and $G_{\text{C.IV}}$ correspond to the pathway where *wingless* is regulated by Cubitus interruptus proteins, while G_{Auto} corresponds to the pathway where *wingless* is regulated by its own protein levels. Thus it is more likely that wild type expression in the segment polarity network is achieved through the Wingless auto-activation pathway. In the absence of the auto-activation link, von Dassow et. al. failed to observe any feasible parameter set in their numerical experiments. However, as soon as the auto-activation pathway was added (the second “missing link” in the model [3]), immediately a significant percentage of feasible parameter sets were observed. This is not surprising, as elucidated by our analysis: while *wingless* auto-activation is not strictly necessary to establishing the segment polarity genes pattern, it does greatly increase the probably that the pattern is achieved (G_{Auto} has a much larger volume, by a factor at least 40, and also exhibits higher robustness indices).

Another fundamental conclusion from the geometry analysis is the existence of six (out of 39) critical parameters which are responsible for 90% of the network failures due to parameter fluctuations. Moreover, the intervals for two of these parameters (κ_{C1prc} and κ_{PTCCI} , Table 7) are independent of parameter space components. The feasible parameter set is thus globally restricted by these parameters, which define “narrow” directions (see Fig. 1 (b)).

Robustness of a regulatory module should not be measured simply as a function of the volume of its admissible parameter space. The geometry (for instance, convexity or existence of sharp points) and topology (connectedness) of the parameter space play fundamental roles in measuring robustness. The analysis developed in this paper can be applied to other systems and regulatory networks, to systematically characterize and explore the admissible space of parameters, its topology and geometry. These provide reliable information on how the network’s interactions contribute to its robustness or fragility, and serve as measures to classify robust regulatory modules.

Acknowledgements

The authors wish to specially thank Adel Dayarian for his careful checking of many computations, as well as the Matlab codes implemented for this paper. We are very grateful for his useful comments and corrections. One of the authors (A.M.S.) thanks Pankaj Mehta for discussions on the segment polarity network that lead to the formulation of the high Hill coefficient version of the model. E.D.S.’s work was partially supported by NSF grant DMS-0614371. A.M.S.’s work was partially supported by a NHGRI grant R01HG03470.

References

- [1] Alon U, Surette MG, Barkai N, Leibler S (1999) Robustness in bacterial chemotaxis. Nature 397:168–171.

- [2] Little J, Shepley D (1999) Robustness of a gene regulatory circuit. *EMBO J* 18:4299–4307.
- [3] von Dassow G, Meir E, Munro E, Odell G (2000) The segment polarity network is a robust developmental module. *Nature* 406:188–192.
- [4] Sengupta A, Djordjevic M, Shraiman B (2002) Specificity and robustness in transcription control network. *Proc Natl Acad Sci USA* 99:2072–2077.
- [5] Savageau M (1971) Parameter sensitivity as a criterion for evaluating and comparing the performance of biochemical systems. *Nature* 229:542–544.
- [6] Heinrich R, Schuster S (1996) *The regulation of cellular systems*. Chapman & Hall, New York.
- [7] Sanson B (2001) Generating patterns from fields of cells. examples from *Drosophila* segmentation. *EMBO Reports* 21:1083–1088.
- [8] Ingolia N (2004) Topology and robustness in the *Drosophila* segment polarity network. *PLoS Biology* 2:0805–0815.
- [9] Albert R, Othmer HG (2003) The topology of the regulatory interactions predicts the expression pattern of the *Drosophila* segment polarity genes. *J Theor Biol* 223:1–18.
- [10] Chaves M, Albert R, Sontag E (2005) Robustness and fragility of boolean models for genetic regulatory networks. *J Theor Biol* 235:431–449.
- [11] Chaves M, Sontag E, Albert R (2006) Methods of robustness analysis for boolean models of gene control networks. *IEE Proc Syst Biol* 153:154–167.
- [12] Ma W, Lai L, Ouyang Q, Tang C (2006) Robustness and modular design of the drosophila segment polarity network. *Mol Syst Biol* 2:70.
- [13] von Dassow G, Odell G (2002) Design and constraints of the *drosophila* segment polarity module: robust spatial patterning emerges from intertwined cell state switches. *J Exp Zool (Mol Dev Evol)* 294:179–215.
- [14] Swantek D, Gergen JP (2004) Ftz modulates runt-dependent activation and repression of segment - polarity gene transcription. *Development* 131:2281–2290.
- [15] Hidalgo A, Ingham PW (1990) Cell patterning in the *Drosophila* segment: spatial regulation of the segment polarity gene *patched*. *Development* 110:291–301.
- [16] Eaton S, Kornberg TB (1990) Repression of *ci-d* in posterior compartments of *drosophila* by *engrailed*. *Genes & Dev* 4:1068–1077.
- [17] Collins GE (1975) Quantifier elimination for real closed fields by cylindrical algebraic decomposition. In: *Second GI Conference on Automata Theory and Formal Languages*, Kaiserslauten, Springer, volume 33 of *Lecture Notes Comp. Sci.* pp. 134–183.
- [18] Arnon DS, Collins GE, McCallum S (1984) Cylindrical algebraic decomposition I: the basic algorithm. *SIAM J Comput* 13:865–877.
- [19] Brown C, Hong H, et al. QEPAD. <http://www.cs.usna.edu/~qepcad/B/QEPCAD.html>.
- [20] Collins GE, Hong H (1991) Partial cylindrical algebraic decomposition in quantifier elimination. *J Symb Comput* 12:299–328.

- [21] Wolfram S (1998) *The Mathematica Book*, 4th ed. Wolfram Media, Cambridge University Press.
- [22] Nesić D, Mareels IMY, Glad ST, Jirstrand M (2001) Software for control system analysis and design, symbol manipulation. In: Webster J, editor, *Encyclopedia of Electrical and Electronics Engineering*, J. Wiley.
- [23] Ghosh R, Tomlin C (2004) Symbolic reachable set computation of piecewise affine hybrid automata and its application to biological modeling: Delta-notch protein signaling. *IEE Trans Syst Biol* 1:170–183.
- [24] Waxman D, Gavrillets S (2005) 20 questions on adaptive dynamics. *J Evol Biol* 18:1139–1154.
- [25] Box G, Muller M (1958) A note on the generation of random normal deviates. *Ann Math Stat* 29:610–611.
- [26] Chaves M, Dayarian A, Sengupta A, Sontag E. Geometry, functionality and robustness: Exploring the parameter space of the segment polarity network. Poster at *The 8th Int. Conf. Systems Biology*, Long Beach, CA, October 2007.

A Notation

The original model can be found in [3, 13]. In order to make our work more clear, we include the notation as well as the original equations below. Without loss of generality (the geometry remains unchanged), each cell is assumed to have four faces (Fig. 2), rather than six as in the original model [3]. The model reproduces a parasegment of four cells and uses repetition of this group of four cells to reproduce the embryo's anterior/posterior axis (A/P axis in Fig. 2), and the circular ventral/dorsal axis (V/D axis in Fig. 2). Because intercellular diffusion is only considered along the A/P axis (left/right), and because cells repeat in the orthogonal V/D direction (up/down), it is indeed equivalent to consider symmetric four-sided or six-sided hexagonal cells.

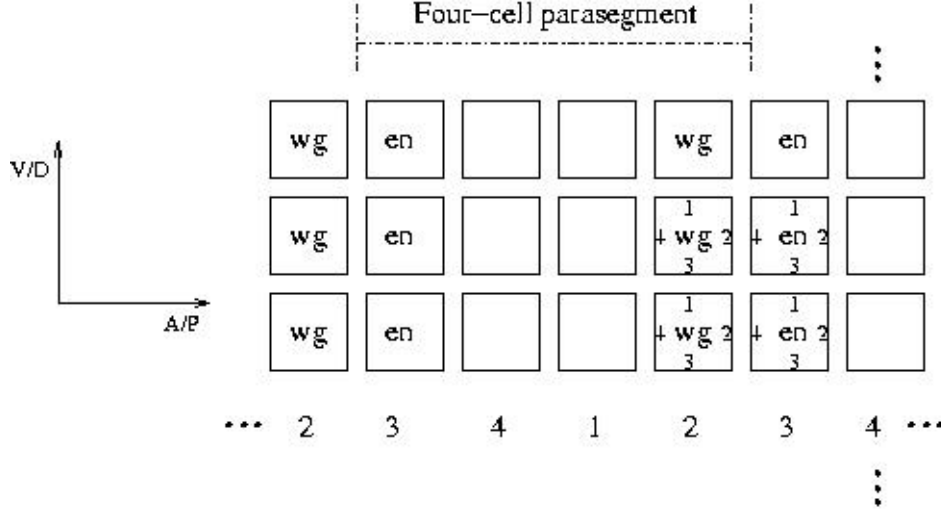


Figure 2: Four cells in a parasegment, with periodic boundary conditions in both dimensions. Each cell has four membranes. The relative values of Wingless in each cell (EWG_i) are shown.

A saturation function, and its horizontal reflexion, are introduced:

$$\begin{aligned}\phi(X, \kappa, \nu) &= \frac{X^\nu}{\kappa^\nu + X^\nu}, \\ \psi(X, \kappa, \nu) &= 1 - \phi(X, \kappa, \nu).\end{aligned}$$

The subscripted variables are as follows:

- X_i = concentration of species X on cell i (when homogeneous throughout the cell),
- $X_{i,j}$ = concentration of species X on cell i , at face j ,
- κ_{XY} = threshold for activation of species Y , induced by species X ,
- $n(i, j)$ = index of neighbor to cell i , at face j ,
- $X_{n(i,j),j+3}$ = concentration of species X on cell face apposite to i, j ,
- $X_{i,T} = \sum_{j=1}^6 X_{i,j}$ = total concentration of species X on cell i ,
- $X_{\underline{i}} = \sum_{j=1}^6 X_{n(i,j),j+3}$ = total concentration of species X presented to cell i by its neighbors.

B Original equations

From [3, 13], the model equations are:

$$\frac{den_i}{dt} = \frac{1}{H_{en}} \left(\phi(\text{EWG}_{\underline{i}}\psi(\text{CN}_i, \kappa_{\text{CNen}}, \nu_{\text{CNen}}), \kappa_{\text{WGen}}, \nu_{\text{WGen}}) - en_i \right) \quad (19)$$

$$\frac{dEN_i}{dt} = \frac{1}{H_{EN}} (en_i - EN_i) \quad (20)$$

$$\frac{dwg_i}{dt} = \frac{1}{H_{wg}} \left(\frac{\alpha_{\text{Clwg}}\phi(\text{CI}_i\psi(\text{CN}_i, \kappa_{\text{CNwg}}, \nu_{\text{CNwg}}), \kappa_{\text{Clwg}}, \nu_{\text{Clwg}}) + \alpha_{\text{WGwg}}\phi(\text{IWG}_i, \kappa_{\text{WGwg}}, \nu_{\text{WGwg}})}{1 + \alpha_{\text{Clwg}}\phi(\text{CI}_i\psi(\text{CN}_i, \kappa_{\text{CNwg}}, \nu_{\text{CNwg}}), \kappa_{\text{Clwg}}, \nu_{\text{Clwg}}) + \alpha_{\text{WGwg}}\phi(\text{IWG}_i, \kappa_{\text{WGwg}}, \nu_{\text{WGwg}})} - wg_i \right) \quad (21)$$

$$\frac{dIWG_i}{dt} = \frac{1}{H_{WG}} (wg_i - IWG_i + r_{\text{endo}}H_{\text{IWG}}\text{EWG}_{i,T} - H_{\text{WG}}r_{\text{exo}}\text{IWG}_i) \quad (22)$$

$$\begin{aligned} \frac{d\text{EWG}_{i,j}}{dt} &= \frac{1}{6}r_{\text{exo}}\text{IWG}_i - r_{\text{endo}}\text{EWG}_{i,j} + r_M(\text{EWG}_{n(i,j),j+3} - \text{EWG}_{i,j}) \\ &\quad + r_{LM}(\text{EWG}_{i,j-1} + \text{EWG}_{i,j+1} - 2\text{EWG}_{i,j}) - \frac{\text{EWG}_{i,j}}{H_{WG}} \end{aligned} \quad (23)$$

$$\frac{dptc_i}{dt} = \frac{1}{H_{ptc}} \left(\phi(\text{CI}_i\psi(\text{CN}_i, \kappa_{\text{CNptc}}, \nu_{\text{CNptc}}), \kappa_{\text{Clptc}}, \nu_{\text{Clptc}}) - ptc_i \right) \quad (24)$$

$$\begin{aligned} \frac{d\text{PTC}_{i,j}}{dt} &= \frac{1}{H_{\text{PTC}}} \left(\frac{1}{6}ptc_i - \text{PTC}_{i,j} - \kappa_{\text{PTCHH}}H_{\text{PTC}}[\text{HH}]_0\text{HH}_{n(i,j),j+3}\text{PTC}_{i,j} \right) \\ &\quad + r_{LM\text{PTC}}(\text{PTC}_{i,j-1} + \text{PTC}_{i,j+1} - 2\text{PTC}_{i,j}) \end{aligned} \quad (25)$$

$$\frac{dci_i}{dt} = \frac{1}{H_{ci}} \left(\phi(B_i\psi(\text{EN}_i, \kappa_{\text{ENci}}, \nu_{\text{ENci}}), \kappa_{\text{Bci}}, \nu_{\text{Bci}}) - ci_i \right) \quad (26)$$

$$\frac{d\text{CI}_i}{dt} = \frac{1}{H_{\text{CI}}} (ci_i - \text{CI}_i - H_{\text{CI}}C_{\text{CI}}\text{CI}_i\phi(\text{PTC}_{i,T}, \kappa_{\text{PTCCI}}, \nu_{\text{PTCCI}})) \quad (27)$$

$$\frac{d\text{CN}_i}{dt} = \frac{1}{H_{\text{CI}}} (H_{\text{CI}}C_{\text{CI}}\text{CI}_i\phi(\text{PTC}_{i,T}, \kappa_{\text{PTCCI}}, \nu_{\text{PTCCI}}) - \text{CN}_i) \quad (28)$$

$$\frac{dhh_i}{dt} = \frac{1}{H_{hh}} \left(\phi(\text{EN}_i\psi(\text{CN}_i, \kappa_{\text{CNhh}}, \nu_{\text{CNhh}}), \kappa_{\text{ENhh}}, \nu_{\text{ENhh}}) - hh_i \right) \quad (29)$$

$$\begin{aligned} \frac{d\text{HH}_{i,j}}{dt} &= \frac{1}{H_{\text{HH}}} \left(\frac{1}{6}hh_i - \text{HH}_{i,j} - \kappa_{\text{PTCHH}}H_{\text{HH}}[\text{PTC}]_0\text{PTC}_{n(i,j),j+3}\text{HH}_{i,j} \right) \\ &\quad + r_{LM\text{HH}}(\text{HH}_{i,j-1} + \text{HH}_{i,j+1} - 2\text{HH}_{i,j}) \end{aligned} \quad (30)$$

C Simplified model, for large ν

$$f_{en_i} = \frac{1}{H_{en}} (\theta(\text{EWG}_i \kappa_{\text{WGen}}) \theta(\kappa_{\text{CNen}} - \text{CN}_i) - en_i) \quad (31)$$

$$f_{\text{EN}_i} = \frac{1}{H_{\text{EN}}} (en_i - \text{EN}_i) \quad (32)$$

$$f_{wg_i} = \frac{1}{H_{wg}} \left(\frac{\alpha_{\text{Clwg}} \theta(\text{CI}_i - \kappa_{\text{Clwg}}) \theta(\kappa_{\text{CNwg}} - \text{CN}_i) + \alpha_{\text{WGwg}} \theta(\text{IWG}_i - \kappa_{\text{WGwg}})}{1 + \alpha_{\text{Clwg}} \theta(\text{CI}_i - \kappa_{\text{Clwg}}) \theta(\kappa_{\text{CNwg}} - \text{CN}_i) + \alpha_{\text{WGwg}} \theta(\text{IWG}_i - \kappa_{\text{WGwg}})} - wg_i \right) \quad (33)$$

$$f_{\text{IWG}_i} = \frac{1}{H_{\text{WG}}} (wg_i - \text{IWG}_i + r_{\text{endo}} H_{\text{IWG}} \text{EWG}_{i,T} - H_{\text{WG}} r_{\text{exo}} \text{IWG}_i) \quad (34)$$

$$f_{\text{EWG}_{i,j}} = \frac{1}{4} r_{\text{exo}} \text{IWG}_i - r_{\text{endo}} \text{EWG}_{i,j} + r_M (\text{EWG}_{n(i,j),j+3} - \text{EWG}_{i,j}) \\ + r_{LM} (\text{EWG}_{i,j-1} + \text{EWG}_{i,j+1} - 2\text{EWG}_{i,j}) - \frac{\text{EWG}_{i,j}}{H_{\text{WG}}} \quad (35)$$

$$f_{ptc_i} = \frac{1}{H_{ptc}} (T_i \theta(\text{CI}_i - \kappa_{\text{Clptc}}) \theta(\kappa_{\text{CNptc}} - \text{CN}_i) - ptc_i) \quad (36)$$

$$f_{\text{PTC}_{i,j}} = \frac{1}{H_{\text{PTC}}} \left(\frac{1}{4} ptc_i - \text{PTC}_{i,j} - \kappa_{\text{PTCHH}} H_{\text{PTC}} [\text{HH}]_0 \text{HH}_{n(i,j),j+3} \text{PTC}_{i,j} \right) \\ + r_{LM\text{PTC}} (\text{PTC}_{i,j-1} + \text{PTC}_{i,j+1} - 2\text{PTC}_{i,j}) \quad (37)$$

$$f_{ci_i} = \frac{1}{H_{ci}} (\theta(B_i - \kappa_{\text{Bci}}) \theta(\kappa_{\text{ENci}} - \text{EN}_i) - ci_i) \quad (38)$$

$$f_{\text{CI}_i} = \frac{1}{H_{\text{CI}}} (ci_i - \text{CI}_i - H_{\text{CI}} C_{\text{CI}} \text{CI}_i \theta(\text{PTC}_{i,T} - \kappa_{\text{PTCCI}})) \quad (39)$$

$$f_{\text{CN}_i} = \frac{1}{H_{\text{CI}}} (H_{\text{CI}} C_{\text{CI}} \text{CI}_i \theta(\text{PTC}_{i,T} - \kappa_{\text{PTCCI}}) - \text{CN}_i) \quad (40)$$

$$f_{hh_i} = \frac{1}{H_{hh}} (\theta(\text{EN}_i - \kappa_{\text{ENhh}}) \psi(\kappa_{\text{CNhh}} - \text{CN}_i) - hh_i) \quad (41)$$

$$f_{\text{HH}_{i,j}} = \frac{1}{H_{\text{HH}}} \left(\frac{1}{4} hh_i - \text{HH}_{i,j} - \kappa_{\text{PTCHH}} H_{\text{HH}} [\text{PTC}]_0 \text{PTC}_{n(i,j),j+3} \text{HH}_{i,j} \right) \\ + r_{LM\text{HH}} (\text{HH}_{i,j-1} + \text{HH}_{i,j+1} - 2\text{HH}_{i,j}) \quad (42)$$

D Steady state pattern

Solving equations (31)-(42) at steady state ($f = 0$), and simplifying where possible, yields the algebraic expressions:

$$en_i = \theta(\text{EWG}_i - \kappa_{\text{WGen}}) \theta(\kappa_{\text{CNe}n} - \text{CN}_i) \quad (43)$$

$$\text{EN}_i = en_i \quad (44)$$

$$wg_i = \frac{\alpha_{\text{CIwg}} \theta(\text{CI}_i - \kappa_{\text{CIwg}}) \theta(\kappa_{\text{CNwg}} - \text{CN}_i) + \alpha_{\text{WGwg}} \theta(\text{IWG}_i - \kappa_{\text{WGwg}})}{1 + \alpha_{\text{CIwg}} \theta(\text{CI}_i - \kappa_{\text{CIwg}}) \theta(\kappa_{\text{CNwg}} - \text{CN}_i) + \alpha_{\text{WGwg}} \theta(\text{IWG}_i - \kappa_{\text{WGwg}})} \quad (45)$$

$$\text{IWG}_i = \frac{H_{\text{IWG}r_{\text{endo}}}}{1 + H_{\text{IWG}r_{\text{exo}}}} \text{EWG}_{i,T} + \frac{1}{1 + H_{\text{IWG}r_{\text{exo}}}} wg_i \quad (46)$$

$$M \text{EWG} = -\frac{1}{4} \frac{r_{\text{exo}}}{1 + H_{\text{IWG}r_{\text{exo}}}} \widetilde{wg} \quad (47)$$

$$ptc_i = T_i \theta(\text{CI}_i - \kappa_{\text{CI}ptc}) \theta(\kappa_{\text{CN}ptc} - \text{CN}_i) \quad (48)$$

$$\begin{aligned} \text{PTC}_{i,j} = & \frac{1}{4} ptc_i - \kappa_{\text{PTCHH}} H_{\text{PTC}} [\text{HH}]_0 \text{HH}_{n(i,j),j+3} \text{PTC}_{i,j} \\ & + r_{LM\text{PTC}} H_{\text{PTC}} (\text{PTC}_{i,j-1} + \text{PTC}_{i,j+1} - 2\text{PTC}_{i,j}) \end{aligned} \quad (49)$$

$$ci_i = U_i \theta(\kappa_{\text{EN}ci} - \text{EN}_i) \quad (50)$$

$$\text{CI}_i = U_i \frac{\theta(\kappa_{\text{EN}ci} - \text{EN}_i)}{1 + H_{\text{CI}} C_{\text{CI}} \theta(\text{PTC}_{i,T} - \kappa_{\text{PTCCI}})} \quad (51)$$

$$\text{CN}_i = U_i \frac{H_{\text{CI}} C_{\text{CI}}}{1 + H_{\text{CI}} C_{\text{CI}}} \theta(\kappa_{\text{EN}ci} - \text{EN}_i) \theta(\text{PTC}_{i,T} - \kappa_{\text{PTCCI}}) \quad (52)$$

$$hh_i = \theta(\text{EN}_i - \kappa_{\text{EN}hh}) \theta(\kappa_{\text{CN}hh} - \text{CN}_i) \quad (53)$$

$$\begin{aligned} \text{HH}_{i,j} = & \frac{1}{4} hh_i - \kappa_{\text{PTCHH}} H_{\text{HH}} [\text{PTC}]_0 \text{PTC}_{n(i,j),j+3} \text{HH}_{i,j} \\ & + r_{LM\text{HH}} H_{\text{HH}} (\text{HH}_{i,j-1} + \text{HH}_{i,j+1} - 2\text{HH}_{i,j}) \end{aligned} \quad (54)$$

EWG is a vector in \mathbb{R}^{16} with components:

$$\text{EWG} = (\text{EWG}_{1,1}, \text{EWG}_{1,2}, \text{EWG}_{1,3}, \text{EWG}_{1,4}, \text{EWG}_{2,1}, \text{EWG}_{2,2}, \text{EWG}_{2,3}, \text{EWG}_{2,4}, \\ \text{EWG}_{3,1}, \text{EWG}_{3,2}, \text{EWG}_{3,3}, \text{EWG}_{3,4}, \text{EWG}_{4,1}, \text{EWG}_{4,2}, \text{EWG}_{4,3}, \text{EWG}_{4,4})'$$

\widetilde{wg} is also a vector in \mathbb{R}^{16} , given by the following Kronecker tensor product

$$\begin{aligned} \widetilde{wg} &= (wg_1, wg_2, wg_3, wg_4)' \times_{kron} (1, 1, 1, 1)' \\ &= (wg_1, wg_1, wg_1, wg_1, wg_2, wg_2, wg_2, wg_2, wg_3, wg_3, wg_3, wg_3, wg_4, wg_4, wg_4, wg_4)' \end{aligned}$$

Putting together the 16 equations (35), and substituting IWG_i by its steady state expression (34), it is not difficult to see that the matrix $M \in \mathbb{R}^{16} \times \mathbb{R}^{16}$ is composed of various 4×4 blocks, as follows:

$$M = \begin{pmatrix} E & F_{24} & 0 & F_{42} \\ F_{42} & E & F_{24} & 0 \\ 0 & F_{42} & E & F_{24} \\ F_{24} & 0 & F_{42} & E \end{pmatrix} \quad (55)$$

where

$$E = \begin{pmatrix} -d & r_{LM} & r_M & r_{LM} \\ r_{LM} & -d & r_{LM} & 0 \\ r_M & r_{LM} & -d & r_{LM} \\ r_{LM} & 0 & r_{LM} & -d \end{pmatrix} + h \begin{pmatrix} 1 & 1 & 1 & 1 \\ 1 & 1 & 1 & 1 \\ 1 & 1 & 1 & 1 \\ 1 & 1 & 1 & 1 \end{pmatrix}$$

with

$$d = H_{IWG}^{-1} + r_{\text{endo}} + r_M + 2r_{LM},$$

$$h = \frac{1}{4} \frac{H_{IWG} r_{\text{exo}}}{1 + H_{IWG} r_{\text{exo}}} r_{\text{endo}}$$

$$F_{24} = \begin{pmatrix} 0 & 0 & 0 & 0 \\ 0 & 0 & 0 & r_M \\ 0 & 0 & 0 & 0 \\ 0 & 0 & 0 & 0 \end{pmatrix}, \quad F_{42} = F'_{24} = \begin{pmatrix} 0 & 0 & 0 & 0 \\ 0 & 0 & 0 & 0 \\ 0 & 0 & 0 & 0 \\ 0 & r_M & 0 & 0 \end{pmatrix}.$$

Note that the steady state equations for EN, IWG, EWG and PTC are algebraic, and in fact exact solutions can be computed from the steady state values of wg and ptc . These are discussed in more detail in the Appendices E and F.

Remark: The parameters are as in [3], except T_i and U_i , which represent the maximal values of ptc and ci (respectively), in each cell. These take values in the interval $[0, 1]$ and generalize the possible ON values of ptc and ci .

Note that, in the simplification from (24) to (36), we have generalized the equation and added distinct maximal levels of expression in each cell, given by T_i ($i = 1, \dots, 4$). This allows a more accurate representation of the experimental, which shows that *patched* is strongly expressed in every second and fourth cells, weakly expressed in every first cell, and not expressed in every third cell (see [3] for more discussion). Thus we will consider the case: $T_1 < T_2 = T_4$.

A similar generalization was made to deal with the activation of *cubitus interruptus*. In von Dassow et. al. model, this is due to some external parameters B_i (not governed by a dynamical equation), with a corresponding activity threshold κ_{Bci} . However, for more generality, and to allow distinct maximal levels of expression in each cell, we have replaced each of the terms $\theta(B_i - \kappa_{Bci})$ in (38) by a parameter U_i , $i = 1, \dots, 4$ (50). Furthermore, in characterizing the set of feasible parameters, it will become clear that allowing distinct U_i enlarges the space of possible parameters, by introducing the four regions $G_{C,I}$ to $G_{C,IV}$.

E Analytically solving Wingless levels

The steady states of Wingless proteins (47) and (46) are given directly by algebraic equations, depending only on wingless mRNA (wg_2) and diffusion parameters for intracellular (membrane-to-membrane) and intercellular communication. Consider equation (47): it is easy to see that M is in fact always invertible (if

all parameters are positive). First note that the matrix is diagonally dominant, by adding up the entries in any column:

$$-(H_{\text{IWG}}^{-1} + r_{\text{endo}} + r_M + 2r_{LM}) + 2r_{LM} + r_M + 4h = -H_{\text{IWG}}^{-1} - r_{\text{endo}} \frac{1}{1 + H_{\text{IWG}} r_{\text{exo}}}$$

which is always a negative quantity. By Geršgorin's Theorem, all eigenvalues of M are contained in the disk centered at $-d + h$ with radius $2r_{LM} + r_M + 3h$, therefore all have negative real parts. Thus, the matrix M is symmetric and negative definite, and since the right-hand-side vector is also non-positive, all solutions are real and positive, *whatever the choice of parameters*. As a fact, note that the vector $\vec{1} = (1, 1, \dots, 1)' \in \mathbb{R}^{16}$ is an eigenvector of M , corresponding to the eigenvalue $\lambda_1 = -H_{\text{IWG}}^{-1} - r_{\text{endo}} \frac{1}{H_{\text{IWG}} + r_{\text{exo}}}$.

Proof of Theorem 2 Assume that $wg = (0, w, 0, 0)$, for any positive constant w . From the symmetry of the matrix equation (47), several facts can be deduced, which lead to the main result (13).

Fact E.1. For all $i = 1, 2, 3, 4$ it holds that

$$\text{EWG}_{i,1} = \text{EWG}_{i,3}.$$

Proof. This is easy to see from the respective equations:

$$\begin{aligned} (-d + h)\text{EWG}_{i,1} + (r_M + h)\text{EWG}_{i,2} + (r_M + h)\text{EWG}_{i,3} + (r_M + h)\text{EWG}_{i,4} &= -\frac{h}{r_{\text{endo}} H_{\text{IWG}}} wg_i \\ (r_M + h)\text{EWG}_{i,1} + (r_M + h)\text{EWG}_{i,2} + (-d + h)\text{EWG}_{i,3} + (r_M + h)\text{EWG}_{i,4} &= -\frac{h}{r_{\text{endo}} H_{\text{IWG}}} wg_i \end{aligned}$$

which can be rearranged to

$$\begin{aligned} -(d + r_M)\text{EWG}_{i,1} + (r_M + h)(\text{EWG}_{i,2} + \text{EWG}_{i,4}) + (r_M + h)(\text{EWG}_{i,3} + \text{EWG}_{i,1}) &= -\frac{h}{r_{\text{endo}} H_{\text{IWG}}} wg_i \\ -(d + r_M)\text{EWG}_{i,3} + (r_M + h)(\text{EWG}_{i,2} + \text{EWG}_{i,4}) + (r_M + h)(\text{EWG}_{i,3} + \text{EWG}_{i,1}) &= -\frac{h}{r_{\text{endo}} H_{\text{IWG}}} wg_i. \end{aligned} \quad (56)$$

Subtracting these two equations yields the desired result. ■

Fact E.2. It holds that

$$\text{EWG}_{2,2} = \text{EWG}_{2,4}, \quad \text{EWG}_{4,2} = \text{EWG}_{4,4}, \quad \text{EWG}_{1,2} = \text{EWG}_{3,4}, \quad \text{EWG}_{1,4} = \text{EWG}_{3,2}.$$

Proof. Exchanging the indexes:

$$2, 2 \leftrightarrow 2, 4 \quad 4, 2 \leftrightarrow 4, 4 \quad 1, 2 \leftrightarrow 3, 4 \quad 1, 4 \leftrightarrow 3, 2$$

it is easy to see that the system remains unchanged (see also Fig. 2). ■

The equality part in (13) is now clear:

Fact E.3. $\text{EWG}_{\underline{1}} = \text{EWG}_{\underline{3}}$.

Proof. We first show that $\text{EWG}_{1,1} = \text{EWG}_{3,3}$. Writing equation (56) for $i = 1$ and $i = 3$:

$$\begin{aligned} -(d + r_M)\text{EWG}_{1,1} + (r_M + h)(\text{EWG}_{1,2} + \text{EWG}_{1,4}) + (r_M + h)(\text{EWG}_{1,3} + \text{EWG}_{1,1}) &= 0 \\ -(d + r_M)\text{EWG}_{3,3} + (r_M + h)(\text{EWG}_{3,2} + \text{EWG}_{3,4}) + (r_M + h)(\text{EWG}_{3,3} + \text{EWG}_{3,1}) &= 0 \end{aligned}$$

Using Fact E.1 one has $\text{EWG}_{1,1} = \text{EWG}_{1,3}$ and $\text{EWG}_{3,1} = \text{EWG}_{3,3}$, and then using Fact E.2 obtains:

$$\begin{aligned} -(d + r_M - 2r_M - 2h)\text{EWG}_{1,1} + (r_M + h)(\text{EWG}_{3,4} + \text{EWG}_{3,2}) &= 0 \\ -(d + r_M - 2r_M - 2h)\text{EWG}_{3,3} + (r_M + h)(\text{EWG}_{3,2} + \text{EWG}_{3,4}) &= 0. \end{aligned}$$

Subtracting these two equations shows that $\text{EWG}_{1,1} = \text{EWG}_{3,3}$. Now recalling the notation for X_i from Appendix A

$$\begin{aligned} \text{EWG}_{\underline{1}} &= \text{EWG}_{1,1} + \text{EWG}_{2,4} + \text{EWG}_{1,3} + \text{EWG}_{4,2} \\ \text{EWG}_{\underline{3}} &= \text{EWG}_{3,1} + \text{EWG}_{4,4} + \text{EWG}_{3,3} + \text{EWG}_{2,2}. \end{aligned}$$

Using $\text{EWG}_{1,1} = \text{EWG}_{3,3}$, Fact E.1 and Fact E.2 obtains:

$$\text{EWG}_{\underline{1}} = \text{EWG}_{3,1} + \text{EWG}_{2,2} + \text{EWG}_{3,3} + \text{EWG}_{4,4} = \text{EWG}_{\underline{3}}.$$

as we wanted to prove. ■

To show the other inequalities, note first that the 16 variables $\text{EWG}_{i,j}$ are thus reduced to only seven:

$$\begin{aligned} E_{1,1} &= \text{EWG}_{1,1} = \text{EWG}_{1,3} = \text{EWG}_{3,1} = \text{EWG}_{3,3} \\ E_{1,2} &= \text{EWG}_{1,2} = \text{EWG}_{3,4} \\ E_{1,4} &= \text{EWG}_{1,4} = \text{EWG}_{3,2} \\ E_{2,1} &= \text{EWG}_{2,1} = \text{EWG}_{2,3} \\ E_{2,2} &= \text{EWG}_{2,2} = \text{EWG}_{2,4} \\ E_{4,1} &= \text{EWG}_{4,1} = \text{EWG}_{4,3} \\ E_{4,2} &= \text{EWG}_{4,2} = \text{EWG}_{4,4} \end{aligned}$$

and satisfy the equations:

$$-(d - r_M - 2h)E_{1,1} + (r_{LM} + h)E_{1,2} + (r_{LM} + h)E_{1,4} = 0 \quad (57)$$

$$2(r_{LM} + h)E_{1,1} - (d - h)E_{1,2} + hE_{1,4} + r_M E_{2,2} = 0 \quad (58)$$

$$2(r_{LM} + h)E_{1,1} + hE_{1,2} - (d - h)E_{1,4} + r_M E_{4,2} = 0 \quad (59)$$

$$-(d - r_M - 2h)E_{2,1} + 2(r_{LM} + h)E_{2,2} = -\frac{h}{r_{\text{endo}}H_{\text{IWG}}}wg_2 \quad (60)$$

$$2(r_{LM} + h)E_{2,1} - (d - 2h)E_{2,2} + r_M E_{1,2} = -\frac{h}{r_{\text{endo}}H_{\text{IWG}}}wg_2 \quad (61)$$

$$-(d - r_M - 2h)E_{4,1} + 2(r_{LM} + h)E_{4,2} = 0 \quad (62)$$

$$2(r_{LM} + h)E_{4,1} - (d - 2h)E_{4,2} + r_M E_{1,4} = 0. \quad (63)$$

To simplify notation, set:

$$A = d - r_M - 2h, \quad B = 2(r_{LM} + h), \quad \bar{w} = \frac{h}{r_{\text{endo}}H_{\text{IWG}}}wg_2,$$

and note that $A > B > 0$.

Fact E.4. The following hold:

(a) $E_{4,1} < E_{4,2} < E_{1,4} < E_{1,2} < E_{2,2}$;

(b) $E_{4,1} < E_{1,1} < E_{1,2}$;

$$(c) \ E_{1,2} + E_{1,4} < E_{2,2} + E_{4,2}$$

Proof. To prove part (a), from eqs. (62), (63) it holds that

$$E_{4,1} = \frac{B}{A}E_{4,2}; \quad E_{4,2} = \frac{r_M A}{A^2 - B^2 + r_M A}E_{1,4}$$

Because $A > B > 0$, it is clear that $E_{4,1} < E_{4,2} < E_{1,4}$. From eqs. (60), (61) it holds that

$$E_{2,1} = \frac{B}{A}E_{2,2} + \frac{1}{A}\bar{w}; \quad E_{2,2} = \frac{r_M A}{A^2 - B^2 + r_M A}E_{1,2} + \frac{A+B}{A^2 - B^2 + r_M A}\bar{w}$$

Then eqs. (58), (59) can be written in the form

$$\begin{aligned} \left(d - r_M \frac{r_M A}{A^2 - B^2 + r_M A} \right) E_{1,2} &= BE_{1,1} + h(E_{1,2} + E_{1,4}) + r_M \frac{A+B}{A^2 - B^2 + r_M A} \bar{w} \\ \left(d - r_M \frac{r_M A}{A^2 - B^2 + r_M A} \right) E_{1,4} &= BE_{1,1} + h(E_{1,2} + E_{1,4}) \end{aligned}$$

which implies that $E_{1,4} < E_{1,2}$ (it is easy to see that the factor multiplying both $E_{1,2}$ and $E_{1,4}$ is positive, since $d > r_M$).

We still need to prove the last inequality in (a), but we can now prove (b). From eq. (57)

$$E_{1,1} = \frac{1}{2} \frac{B}{A} (E_{1,2} + E_{1,4}) < E_{1,2}$$

using (a) and because $B < A$. This proves the second inequality in (b). To prove (c), substitute this $E_{1,1}$ expression into the sum of eqs. (58), (59):

$$E_{2,2} + E_{4,2} = \frac{A^2 - B^2 + r_M A}{r_M A} (E_{1,2} + E_{1,4}) > E_{1,2} + E_{1,4}.$$

The last part of (a) now follows from (c) together with $E_{4,2} < E_{1,4}$, which implies $E_{1,2} < E_{2,2}$.

Finally, the first part of (b) is easy to see from:

$$E_{1,1} - E_{4,1} = \frac{1}{2} \frac{B}{A} (E_{1,2} + E_{1,4}) - \frac{B}{A} E_{4,2} > \frac{1}{2} \frac{B}{A} (E_{1,2} + E_{1,4} - E_{1,4}) > 0.$$

■

To prove the first inequality of Theorem 2 is now straightforward.

Fact E.5. $\text{EWG}_4 < \text{EWG}_1$

Proof. Recall the notation for EWG_i and use Fact E.4

$$\begin{aligned} \text{EWG}_1 - \text{EWG}_4 &= 2E_{1,1} + E_{2,2} + E_{4,2} - 2E_{4,1} - 2E_{1,4} \\ &= 2(E_{1,1} - E_{4,1}) + (E_{2,2} + E_{4,2} - E_{1,2} - E_{1,4}) + (E_{1,2} - E_{1,4}) > 0. \end{aligned}$$

■

The next result finishes the proof of Theorem 2.

Fact E.6. $\text{EWG}_3 < \text{EWG}_2$

Proof. Consider:

$$\begin{aligned} \text{EWG}_2 - \text{EWG}_1 &= 2E_{2,1} + 2E_{1,2} - 2E_{1,1} - E_{2,2} - E_{4,2} \\ &= 2(E_{1,2} - E_{1,1}) + (E_{2,1} - E_{2,2}) + (E_{2,1} - E_{4,2}), \end{aligned}$$

which is positive if $E_{2,1} > E_{2,2}$. We will show that this is indeed the case. It will be useful to see that

$$E_{1,2} = r_M \frac{A+B}{d(A^2 - B^2 + r_M A) - r_M^2 A} \bar{w} + \frac{1}{2} r_M \frac{A^2 - B^2 + r_M A}{d(A^2 - B^2 + r_M A) - r_M^2 A} \frac{-A^2 + B^2 + (d - r_M)A}{(A-B)(A^2 - B^2 + 2r_M A)} \bar{w}.$$

Now consider

$$E_{2,1} - E_{2,2} = -\frac{A-B}{A} \frac{r_M A}{A^2 - B^2 + r_M A} E_{1,2} - \frac{A-B}{A} \frac{A+B}{A^2 - B^2 + r_M A} \bar{w} + \frac{1}{A} \bar{w}.$$

The last two terms can be combined into

$$\frac{r_M}{A^2 - B^2 + r_M A} \bar{w},$$

and the two terms due to $E_{1,2}$ can be simplified to:

$$-r_M \frac{1}{A^2 - B^2 + r_M A} \frac{(A-B)(A+B)}{\frac{d}{r_M}(A^2 - B^2 + r_M A) - r_M A} \bar{w}$$

and

$$-\frac{r_M}{2} \frac{1}{A^2 - B^2 + 2r_M A} \frac{-A^2 + B^2 + (d - r_M)A}{\frac{d}{r_M}(A^2 - B^2 + r_M A) - r_M A} \bar{w}.$$

Factoring out $r_M \bar{w} / (\frac{d}{r_M}(A^2 - B^2 + r_M A) - r_M A)$, one obtains

$$\begin{aligned} \frac{1}{r_M \bar{w}} \frac{d}{r_M} (A^2 - B^2 + r_M A) - r_M A (E_{2,1} - E_{2,2}) &= \\ \frac{1}{A^2 - B^2 + r_M A} \left(\frac{d}{r_M} (A^2 - B^2 + r_M A) - r_M A - (A^2 - B^2) \right) &- \frac{1}{2} \frac{-A^2 + B^2 + (d - r_M)A}{A^2 - B^2 + 2r_M A} \end{aligned}$$

which can be further simplified to

$$\left(\frac{\frac{d}{r_M} - 1}{A^2 - B^2 + r_M A} \right) (A^2 - B^2) + \frac{1}{2} \frac{A^2 - B^2}{A^2 - B^2 + 2r_M A} + \frac{(d - r_M)A}{A^2 - B^2 + r_M A} - \frac{1}{2} \frac{(d - r_M)A}{A^2 - B^2 + 2r_M A} > 0$$

because the first two terms are clearly positive, and the last two terms add up to a positive number. This shows that $E_{2,1} > E_{2,2}$, as we wanted to prove. \blacksquare

F Analytically solving PTC and HH levels

In this section, we prove uniqueness of solutions for PTC and HH in the conditions of Theorem 1. The steady state levels of Patched and Hedgehog proteins are given by a system of nonlinear equations (49) and (54). These equations can be solved explicitly and uniquely in the case $ptc_2 = ptc_4 = T_2$, which is true is the steady state output is in \mathcal{Y}^{WT} . To simplify notation, we use

$$r_P = r_{LM\text{PTC}}, \quad r_H = r_{LM\text{HH}}, \quad \kappa_H = \kappa_{\text{PTCHH}}[\text{HH}]_0, \quad \kappa_P = \kappa_{\text{PTCHH}}[\text{PTC}]_0,$$

and define

$$d_P = \frac{1}{H_{\text{PTC}}} + 2r_P, \quad d_H = \frac{1}{H_{\text{HH}}} + 2r_H.$$

We introduce further notation:

$$\beta_P = \frac{2r_P^2 d_P}{d_P^2 - 2r_P^2}, \quad \gamma_P = \frac{1}{4H_{\text{PTC}}} + \frac{1}{4H_{\text{PTC}}} \frac{2r_P(r_P + d_P)}{d_P^2 - 2r_P^2} = \frac{1}{4H_{\text{PTC}}} \frac{d_P(2r_P + d_P)}{d_P^2 - 2r_P^2}.$$

Lemma F.1. Let $x \in \mathcal{W}$ be such that $h(x) \in \mathcal{Y}^{\text{WT}}$. Then, the solution for HH is:

$$\begin{aligned} \text{HH}_{i,1} = \text{HH}_{i,2} = \text{HH}_{i,3} = \text{HH}_{i,4} &= 0, \quad i = 1, 2, 4, \\ \text{HH}_{3,2} = \text{HH}_{3,4} &= \text{Root}_+, \\ \text{HH}_{3,1} = \text{HH}_{3,3} &= \frac{1}{d_H} \left(\frac{1}{4} \frac{hh_3}{H_{\text{HH}}} + r_H \text{HH}_{3,2} + r_H \text{HH}_{3,4} \right), \end{aligned}$$

where Root_+ is the positive root of the quadratic equation:

$$\begin{aligned} k_H(d_H^2 - 4r_H^2)X^2 + \left((d_P - \beta_P)(d_H^2 - 4r_H^2) - k_H(d_H + 2r_H) \frac{hh_3}{4H_{\text{HH}}} + d_H k_P \gamma_P \text{ptc}_2 \right) X \\ - (d_P - \beta_P)(d_H + 2r_H) \frac{hh_3}{4H_{\text{HH}}} = 0. \end{aligned}$$

And the solution for PTC is:

$$\begin{aligned} \text{PTC}_{3,1} = \text{PTC}_{3,2} = \text{PTC}_{3,3} = \text{PTC}_{3,4} &= 0, \\ \text{PTC}_{2,2} = \text{PTC}_{4,4} &= \frac{\gamma_P T_2}{d_P - \beta_P + k_H \text{HH}_{3,4}}, \\ \text{PTC}_{2,1} = \text{PTC}_{2,3} = \text{PTC}_{4,1} = \text{PTC}_{4,3} &= \frac{1}{d_P^2 - 2r_P^2} \left(r_P d_P \text{PTC}_{2,2} + \frac{1}{4H_{\text{PTC}}} (d_P + r_P) T_2 \right), \\ \text{PTC}_{2,4} = \text{PTC}_{4,2} &= \frac{1}{d_P} \left(\frac{1}{4} \frac{T_2}{H_{\text{PTC}}} + 2r_P \text{PTC}_{2,1} \right). \end{aligned}$$

Proof. Let $x \in \mathcal{W}$ and $h(x)$ be a vector in \mathcal{Y}^{WT} , defined by (7). Because *hedgehog* is not expressed in cells 1, 2 and 4, note that for $i = 1, 2, 4$

$$\begin{aligned} \text{HH}_{i,T} = \sum_{j=1}^4 \text{HH}_{i,j} &= hh_i - \kappa_P(\dots) + r_H \sum_{j=1}^4 (\text{HH}_{i,j-1} + \text{HH}_{i,j-1} - 2\text{HH}_{i,j}) \\ &= -\kappa_P(\dots) \end{aligned}$$

since $hh = (0, 0, 1, 0)$, and the sum that multiplies r_H cancels out. The terms in $\kappa_P(\dots)$ are all nonnegative, and therefore they can only be zero. We conclude that:

$$\text{HH}_{i,1} = \text{HH}_{i,2} = \text{HH}_{i,3} = \text{HH}_{i,4} = 0, \quad i = 1, 2, 4.$$

A similar argument shows that $\text{ptc}_3 = 0$ implies:

$$\text{PTC}_{3,1} = \text{PTC}_{3,2} = \text{PTC}_{3,3} = \text{PTC}_{3,4} = 0.$$

Therefore, the only nonlinear terms appear in the equations for $PTC_{2,2}$ and $PTC_{4,4}$:

$$\begin{aligned} d_P PTC_{2,2} - r_P PTC_{2,1} - r_P PTC_{2,3} + \kappa_H PTC_{2,2} HH_{3,4} &= \frac{1}{4H_{PTC}} ptc_2 \\ d_P PTC_{4,4} - r_P PTC_{4,1} - r_P PTC_{4,3} + \kappa_H PTC_{4,4} HH_{3,2} &= \frac{1}{4H_{PTC}} ptc_4. \end{aligned}$$

Moreover, symmetry of the system shows that $PTC_{2,1} = PTC_{2,3}$ and $PTC_{4,1} = PTC_{4,3}$, because each pair satisfies exactly the same equation:

$$d_P PTC_{2,1} - r_P PTC_{2,2} - r_P PTC_{2,4} = \frac{1}{4H_{PTC}} ptc_2 \quad (64)$$

$$d_P PTC_{4,3} - r_P PTC_{4,4} - r_P PTC_{4,2} = \frac{1}{4H_{PTC}} ptc_4. \quad (65)$$

We then have:

$$\begin{aligned} PTC_{2,4} &= \frac{1}{d_P} \left(\frac{1}{4H_{PTC}} ptc_2 + 2r_P PTC_{2,1} \right) \\ PTC_{4,2} &= \frac{1}{d_P} \left(\frac{1}{4H_{PTC}} ptc_4 + 2r_P PTC_{4,1} \right). \end{aligned}$$

Solving for $PTC_{2,1}$ as a function of $PTC_{2,2}$, and for $PTC_{4,1}$ as a function of $PTC_{4,4}$:

$$\begin{aligned} PTC_{2,1} &= \frac{1}{d_P^2 - 2r_P^2} \left(r_P d_P PTC_{2,2} + \frac{1}{4H_{PTC}} (d_P + r_P) ptc_2 \right) \\ PTC_{4,1} &= \frac{1}{d_P^2 - 2r_P^2} \left(r_P d_P PTC_{4,4} + \frac{1}{4H_{PTC}} (d_P + r_P) ptc_4 \right). \end{aligned}$$

Thus we get equations depending only on $PTC_{2,2}$ and $HH_{3,4}$, and on $PTC_{4,4}$ and $HH_{3,2}$:

$$d_P PTC_{2,2} - \frac{2r_P}{d_P^2 - 2r_P^2} \left(r_P d_P PTC_{2,2} + \frac{1}{4H_{PTC}} (d_P + r_P) ptc_2 \right) + \kappa_H PTC_{2,2} HH_{3,4} = \frac{1}{4H_{PTC}} ptc_2 \quad (66)$$

$$d_P PTC_{4,4} - \frac{2r_P}{d_P^2 - 2r_P^2} \left(r_P d_P PTC_{4,4} + \frac{1}{4H_{PTC}} (d_P + r_P) ptc_4 \right) + \kappa_H PTC_{4,4} HH_{3,2} = \frac{1}{4H_{PTC}} ptc_4. \quad (67)$$

On the other hand, since $PTC_{3,j} = 0$ for all j , it follows that:

$$HH_{3,1} = HH_{3,3} = \frac{1}{d_H} \left(\frac{1}{4H_{HH}} hh_3 + r_H HH_{3,2} + r_H HH_{3,4} \right),$$

and substituting into the $HH_{3,4}$ and $HH_{3,2}$ equations:

$$d_H HH_{3,4} - 2 \frac{r_H}{d_H} \left(\frac{1}{4H_{HH}} hh_3 + r_H HH_{3,2} + r_H HH_{3,4} \right) - \kappa_P PTC_{2,2} HH_{3,4} = \frac{1}{4H_{HH}} hh_3 \quad (68)$$

$$d_H HH_{3,2} - 2 \frac{r_H}{d_H} \left(\frac{1}{4H_{HH}} hh_3 + r_H HH_{3,2} + r_H HH_{3,4} \right) - \kappa_P PTC_{4,4} HH_{3,2} = \frac{1}{4H_{HH}} hh_3. \quad (69)$$

The last four equations may be solved for the four variables $PTC_{2,2}$, $PTC_{4,4}$, $HH_{3,2}$ and $HH_{3,4}$, and the remaining PTC , HH will then follow. Recalling the notation introduced above, one can write

$$PTC_{2,2} = \frac{\gamma_P ptc_2}{d_P - \beta_P + k_H HH_{3,4}}, \quad PTC_{4,4} = \frac{\gamma_P ptc_4}{d_P - \beta_P + k_H HH_{3,2}}. \quad (70)$$

This leads to

$$\begin{aligned} d_H HH_{3,4} - 2 \frac{r_H}{d_H} \left(\frac{1}{4H_{HH}} hh_3 + r_H HH_{3,2} + r_H HH_{3,4} \right) - \kappa_P \gamma_P ptc_2 \frac{HH_{3,4}}{d_P - \beta_P + k_H HH_{3,4}} &= \frac{1}{4H_{HH}} hh_3 \\ d_H HH_{3,2} - 2 \frac{r_H}{d_H} \left(\frac{1}{4H_{HH}} hh_3 + r_H HH_{3,2} + r_H HH_{3,4} \right) - \kappa_P \gamma_P ptc_4 \frac{HH_{3,2}}{d_P - \beta_P + k_H HH_{3,2}} &= \frac{1}{4H_{HH}} hh_3. \end{aligned}$$

From the symmetry of these equations, it is easy to see that

$$ptc_2 = ptc_4 \quad \Rightarrow \quad HH_{3,4} = HH_{3,2}.$$

and thus have the following equation for $HH_{3,4} = HH_{3,2} = X$ (after some simple algebra steps):

$$\begin{aligned} k_H (d_H^2 - 4r_H^2) X^2 + \left((d_P - \beta_P)(d_H^2 - 4r_H^2) - k_H (d_H + 2r_H) \frac{hh_3}{4H_{HH}} + d_H k_P \gamma_P ptc_2 \right) X \\ - (d_P - \beta_P)(d_H + 2r_H) \frac{hh_3}{4H_{HH}} = 0. \end{aligned} \quad (71)$$

We next show that only one of the two roots of this second order polynomial is positive and hence the unique solution to $HH_{3,2}$, $HH_{3,4}$. Let the polynomial be of the form $c_2 X^2 + c_1 X + c_0 = 0$. The term inside the square root will be $c_1^2 - 4c_0 c_2$ where:

$$-4c_0 c_2 = 4k_H (d_H^2 - 4r_H^2)(d_P - \beta_P)(d_H + 2r_H) \frac{hh_3}{4H_{HH}}.$$

The factor $d_H^2 - 4r_H^2$ is positive, by definition of d_H . The factor

$$d_P - \beta_P = d_P - \frac{2r_P^2 d_P}{d_P^2 - 2r_P^2} = d_P (d_P^2 - 4r_P^2)$$

is also positive, again by definition of d_P . This means that $c_1^2 - 4c_0 c_2 > c_1^2$, so whatever the sign of c_1 , $-c_1 - \sqrt{c_1^2 - 4c_0 c_2} < 0$, which leaves us with:

$$HH_{3,2} = HH_{3,4} = \frac{-c_1 + \sqrt{c_1^2 - 4c_0 c_2}}{2c_2}$$

(the coefficients are as in (71)). ■

F.1 Asymmetry in patched ON levels

The assumption $T_2 = T_4$ is now relaxed, and the more general case is analyzed. The main question is how Patched asymmetry influences the space of parameters, G , and whether the five components can become connected. In other words, does the more general case assumption $T_2 \neq T_4$ leads to a increasing network robustness. It will be seen that this is actually not true. The presence of CN in the first cell is still necessary (because Wingless protein expression is not affected by ptc levels), but expression of CN in the second and fourth cells may now be different. While it is now difficult to explicitly solve the nonlinear equations for PTC_i and HH_i , it can still be shown that $ptc_2 < ptc_4$ implies $PTC_2 < PTC_4$.

Fact F.1. $(ptc_2 - ptc_4)(PTC_2 - PTC_4) > 0$.

Proof. To see this assume that $ptc_2 > ptc_4$ (the opposite case follows a similar argument). From the discussion above, the Hedgehog values must satisfy

$$d_H HH_{3,4} - a_1 ptc_2 \frac{HH_{3,4}}{a_2 + a_3 HH_{3,4}} = d_H HH_{3,2} - a_1 ptc_4 \frac{HH_{3,2}}{a_2 + a_3 HH_{3,2}} \quad (72)$$

with some positive constants $a_{1,2,3}$. Because this is an increasing function of $HH_{\cdot,\cdot}$, and decreasing with ptc_{\cdot} , it follows that $HH_{3,4} > HH_{3,2}$. Rewriting (72)

$$HH_{3,4} \left(d_H - a_1 ptc_2 \frac{1}{a_2 + a_3 HH_{3,4}} \right) = HH_{3,2} \left(d_H - a_1 ptc_4 \frac{1}{a_2 + a_3 HH_{3,2}} \right)$$

and comparing with the Patched values from (66),

$$\frac{HH_{3,4} d_H - a_0 PTC_{4,4}}{HH_{3,2} d_H - a_0 PTC_{2,2}} > 1$$

for an appropriate positive constant a_0 . This last inequality shows that $PTC_{2,2} > PTC_{4,4}$. Finally, retracing back to (64), it is not difficult to see that

$$ptc_2 > ptc_4 \Rightarrow PTC_{2,T} > PTC_{4,T}.$$

■

Distinct ptc_2, ptc_4 does not increase robustness On the whole, there are four possibilities to consider: (i) $PTC_{2,4} > \kappa_{PTCCI}$; (ii) $PTC_2 > \kappa_{PTCCI} > PTC_4$; (iii) $PTC_4 > \kappa_{PTCCI} > PTC_2$; and (iv) $\kappa_{PTCCI} > PTC_{2,4}$. As already mentioned, $PTC_1 > \kappa_{PTCCI}$ in all four situations.

Situation (i) is similar to the case $T_2 = T_4$ already studied, where CI and CN have the form (14). In case (ii), the Cubitus proteins have the form:

$$\begin{aligned} CI_{1,2} &= U_{1,2} \frac{1}{1 + H_{CI} C_{CI}}, & CN_{1,2} &= U_{1,2} \frac{H_{CI} C_{CI}}{1 + H_{CI} C_{CI}} \\ CI_4 &= U_4, & CN_4 &= 0. \end{aligned}$$

The conditions for wg activation by CI in the second cell require $U_2 > U_4$, so the parameters κ_{CIwg} , κ_{CNwg} may take values only from components $G_{C,I}$ or $G_{C,II}$, or G_{Auto} . In case (iii) the Cubitus repressor protein is not present in the second cell:

$$\begin{aligned} CI_{1,4} &= U_{1,4} \frac{1}{1 + H_{CI} C_{CI}}, & CN_{1,4} &= U_{1,4} \frac{H_{CI} C_{CI}}{1 + H_{CI} C_{CI}} \\ CI_2 &= U_2, & CN_2 &= 0. \end{aligned}$$

Since $CN_2 = 0$, repression of *engrailed* on the second cell must now be due to insufficient Wingless activation, implying:

$$EWG_2 < \kappa_{WGen} < EWG_3$$

which is impossible, since it was shown that $EWG_2 > EWG_3$ for any choice of parameters (see Appendix E). Finally, in case (iv), Cubitus repressor protein is not present in either the second or fourth cells:

$$\begin{aligned} CI_1 &= U_1 \frac{1}{1 + H_{CI} C_{CI}}, & CN_1 &= U_1 \frac{H_{CI} C_{CI}}{1 + H_{CI} C_{CI}} \\ CI_{2,4} &= U_{2,4}, & CN_{2,4} &= 0. \end{aligned}$$

Again it is not difficult to see that κ_{CIwg} , κ_{CNwg} may take values only from components $G_{C,I}$ or $G_{C,II}$, or G_{Auto} (it is always necessary that $U_2 > U_4$).

Component G_{Auto} will never become connected to any of the other four, due to opposite requirements on the second cell (compare equations (16) and (17)). But the comparison above for CI_i and CN_i show that the more general case $T_2 \neq T_4$ only contributes to connect components $G_{C,I}$ and $G_{C,II}$, all the others remaining disconnected.

G Computing the cylindrical algebraic decomposition

A CAD for the parameter space G can be computed from equations (53)-(54), by imposing the conditions $h(x) \in \mathcal{Y}^{\text{WT}}$, as given by (11). By Theorem 1, given $h(x)$ we can solve for EN, EWG, IWG, PTC, and HH uniquely as a function of en, wg, ptc, hh and the parameters p .

First, note that a CAD is not unique, and here we will start by arbitrarily choosing the maximal levels for wg, ci , and ptc , that is:

$$\alpha_{\text{CIwg}}, \alpha_{\text{IWGwg}}, U_1, U_2, U_4, T_2, T_1 \quad (\text{with } T_1 < T_2), \quad (73)$$

with physiological constraints as listed in Table 6. A hierarchy of conditions can then be computed for the remaining parameters.

Second, note that the parameters appearing on the equations for IWG and EWG, as well as those for PTC and HH, do not appear on any other equation and, moreover, the unique solution for these four species has the same form for any set of parameters (Theorem 1). Similarly, all half lives and the Cubitus cleavage rate can also be arbitrarily chosen. So, we have a second group of parameters which can be arbitrarily chosen, with no conditions to satisfy except for physiological constraints. These parameters are (also listed in Table 6):

$$\begin{aligned} &H_{\text{WG}}, r_M, r_{LM}, r_{\text{endo}}, r_{\text{exo}}, \\ &H_{\text{PTC}}, H_{\text{HH}}, [\text{PTC}]_0, [\text{HH}]_0, r_{LM\text{PTC}}, r_{LM\text{HH}}, \kappa_{\text{PTCHH}}, \\ &H_{\text{CI}}, C_{\text{CI}}. \end{aligned} \quad (74)$$

Let $p_{r_{\text{free}}}$ denote the subfamily of parameters (73) and (74).

Third, using the computed unique steady state expressions for EN, IWG, EWG, PTC, HH, CI, and CN write down the conditions for consistency for the expressions of en, wg, ptc, ci , and hh . We have seen that EN, CI, and CN have simple expressions:

$$\text{EN}^{\text{WT}} = en^{\text{WT}} = (0, 0, 1, 0)' \quad (75)$$

and, from Lemma 2.2,

$$\begin{aligned} \text{CI}^{\text{WT}} &= \frac{1}{1 + H_{\text{CI}}C_{\text{CI}}}(U_1, U_2, 0, U_4), \\ \text{CN}^{\text{WT}} &= \frac{H_{\text{CI}}C_{\text{CI}}}{1 + H_{\text{CI}}C_{\text{CI}}}(U_1, U_2, 0, U_4). \end{aligned}$$

The steady state expressions for IWG, EWG, PTC, and HH are more complicated so, for simplicity, we will denote them:

$$\begin{aligned} \text{EWG} &= F_{\text{EWG}} = F_{\text{EWG}}(p_{r_{\text{free}}}), \\ \text{IWG} &= F_{\text{IWG}} = F_{\text{IWG}}(p_{r_{\text{free}}}), \\ \text{PTC} &= F_{\text{PTC}} = F_{\text{PTC}}(p_{r_{\text{free}}}), \\ \text{HH} &= F_{\text{HH}} = F_{\text{HH}}(p_{r_{\text{free}}}). \end{aligned}$$

We start by showing that there are other parameters which can be arbitrarily chosen, and thus complete the proof of Table 6.

Lemma G.1. The parameters $\kappa_{\text{ENci}}, \kappa_{\text{ENhh}}$, and κ_{CNhh} may take arbitrary values in the interval $(0, 1)$.

Proof. The requirements for consistency of the ci^{WT} expression are:

$$\text{EN}_1^{\text{WT}} < \kappa_{\text{ENci}} \text{ and } \text{EN}_2^{\text{WT}} < \kappa_{\text{ENci}} \text{ and } \text{EN}_3^{\text{WT}} > \kappa_{\text{ENci}} \text{ and } \text{EN}_4^{\text{WT}} < \kappa_{\text{ENci}},$$

which are clearly satisfied, in view of (75), for any $\kappa_{\text{ENci}} \in (0, 1)$. The requirements for consistency of the hh^{WT} expression are:

$$\begin{aligned} \text{EN}_1^{\text{WT}} < \kappa_{\text{ENhh}} \quad \boxed{\text{or}} \quad U_1 \frac{H_{\text{Cl}}C_{\text{Cl}}}{1 + H_{\text{Cl}}C_{\text{Cl}}} > \kappa_{\text{CNhh}} \\ \text{EN}_2^{\text{WT}} < \kappa_{\text{ENhh}} \quad \boxed{\text{or}} \quad U_2 \frac{H_{\text{Cl}}C_{\text{Cl}}}{1 + H_{\text{Cl}}C_{\text{Cl}}} > \kappa_{\text{CNhh}} \\ \text{EN}_3^{\text{WT}} > \kappa_{\text{ENhh}} \quad \text{and} \quad 0 < \kappa_{\text{CNhh}} \\ \text{EN}_4^{\text{WT}} < \kappa_{\text{ENhh}} \quad \boxed{\text{or}} \quad U_4 \frac{H_{\text{Cl}}C_{\text{Cl}}}{1 + H_{\text{Cl}}C_{\text{Cl}}} > \kappa_{\text{CNhh}} \end{aligned}$$

Again in view of (75), these conditions are all automatically satisfied for any $\kappa_{\text{ENhh}}, \kappa_{\text{CNhh}} \in (0, 1)$. ■

Next, the constraints for the parameters in Table 7 are shown.

Lemma G.2. For system (1) with steady state output set (11), the following hold:

- (a) $\kappa_{\text{PTCCI}} \in (0, \min\{T_1, \text{PTC}_{2,\text{T}}\})$;
- (b) $\kappa_{\text{Clptc}} \in (0, \frac{1}{1+H_{\text{Cl}}C_{\text{Cl}}} \min\{U_1, U_2, U_4\})$;
- (c) $\kappa_{\text{CNptc}} \in (\frac{H_{\text{Cl}}C_{\text{Cl}}}{1+H_{\text{Cl}}C_{\text{Cl}}} \max\{U_1, U_2, U_4\}, 1)$;
- (d) Either $\kappa_{\text{CNen}} \in (0, \frac{H_{\text{Cl}}C_{\text{Cl}}}{1+H_{\text{Cl}}C_{\text{Cl}}} \min\{U_1, U_2, U_4\})$ and $\kappa_{\text{WGen}} \in (0, \text{EWG}_3)$,
or $\kappa_{\text{CNen}} \in (0, \frac{H_{\text{Cl}}C_{\text{Cl}}}{1+H_{\text{Cl}}C_{\text{Cl}}} \min\{U_1, U_2\})$ and $\kappa_{\text{WGen}} \in (\text{EWG}_4, \text{EWG}_3)$.

Proof. Part (a) follows immediately from Lemma 2.2, since $\text{PTC}_1^{\text{WT}} = T_1$ and both $\text{PTC}_{1,2}^{\text{WT}}$ have to be larger than κ_{PTCCI} .

To prove parts (b) and (c), consider the requirements for consistency of the ptc^{WT} expression:

$$\begin{aligned} U_1 \frac{1}{1 + H_{\text{Cl}}C_{\text{Cl}}} > \kappa_{\text{Clptc}} \quad \text{and} \quad U_1 \frac{H_{\text{Cl}}C_{\text{Cl}}}{1 + H_{\text{Cl}}C_{\text{Cl}}} < \kappa_{\text{CNptc}} \\ U_2 \frac{1}{1 + H_{\text{Cl}}C_{\text{Cl}}} > \kappa_{\text{Clptc}} \quad \text{and} \quad U_2 \frac{H_{\text{Cl}}C_{\text{Cl}}}{1 + H_{\text{Cl}}C_{\text{Cl}}} < \kappa_{\text{CNptc}} \\ 0 < \kappa_{\text{Clptc}} \quad \boxed{\text{or}} \quad 0 > \kappa_{\text{CNptc}} \\ U_4 \frac{1}{1 + H_{\text{Cl}}C_{\text{Cl}}} > \kappa_{\text{Clptc}} \quad \text{and} \quad U_4 \frac{H_{\text{Cl}}C_{\text{Cl}}}{1 + H_{\text{Cl}}C_{\text{Cl}}} < \kappa_{\text{CNptc}}. \end{aligned}$$

The third line is trivially satisfied, while the other lines involve logical ANDs. These immediately yield conditions (b) and (c).

To prove part (d), consider the requirements for consistency of the en^{WT} expression:

$$\begin{aligned} F_{\text{EWG}_1} < \kappa_{\text{WGen}} \quad \boxed{\text{or}} \quad U_1 \frac{H_{\text{Cl}}C_{\text{Cl}}}{1 + H_{\text{Cl}}C_{\text{Cl}}} > \kappa_{\text{CNen}} \\ F_{\text{EWG}_2} < \kappa_{\text{WGen}} \quad \boxed{\text{or}} \quad U_2 \frac{H_{\text{Cl}}C_{\text{Cl}}}{1 + H_{\text{Cl}}C_{\text{Cl}}} > \kappa_{\text{CNen}} \\ F_{\text{EWG}_3} > \kappa_{\text{WGen}} \quad \text{and} \quad 0 < \kappa_{\text{CNen}} \\ F_{\text{EWG}_4} < \kappa_{\text{WGen}} \quad \boxed{\text{or}} \quad U_4 \frac{H_{\text{Cl}}C_{\text{Cl}}}{1 + H_{\text{Cl}}C_{\text{Cl}}} > \kappa_{\text{CNen}}. \end{aligned}$$

Theorem 2, says that $F_{EWG4} < F_{EWG1} = F_{EWG3} < F_{EWG2}$, so these conditions can be reduced to:

$$\kappa_{WGen} < F_{EWG3} \quad \text{and} \quad \kappa_{CNen} < \frac{H_{Cl}C_{Cl}}{1 + H_{Cl}C_{Cl}} \min\{U_1, U_2, U_4\}, \quad (76)$$

or

$$F_{EWG4} < \kappa_{WGen} < F_{EWG3} \quad \text{and} \quad \kappa_{CNen} < \frac{H_{Cl}C_{Cl}}{1 + H_{Cl}C_{Cl}} \min\{U_1, U_2\}. \quad (77)$$

It is obvious that the subsets defined by (76) and (77) intersect: just choose elements $\kappa_{WGen} \in (F_{EWG4}, F_{EWG3})$ and $\kappa_{CNen} < \frac{H_{Cl}C_{Cl}}{1 + H_{Cl}C_{Cl}} \min\{U_1, U_2, U_4\}$. ■

Lastly, we come to the parameters in Table 8 and which complete the characterization of the feasible parameter space.

Theorem 4. *The set G consists of five disconnected regions of parameters:*

$$G = G_{C,I} \cup G_{C,II} \cup G_{C,III} \cup G_{C,IV} \cup G_{Auto}$$

each of the regions characterized by Tables 6, 7, 8.

Proof. The only parameters whose possible intervals have not yet been found are κ_{WGwg} , κ_{Clwg} , and κ_{CNwg} . Consider now the requirements for consistency of the wg^{WT} expression. There are three distinct cases, depending on whether activation of wg is autocatalytic, or through the CI pathway, or through both.

Case 1: both CI and IWG contribute to activation of wg . Here $wg_2^{WT} = \frac{\alpha_{Clwg} + \alpha_{WGwg}}{1 + \alpha_{Clwg} + \alpha_{WGwg}}$, so set $F_{IWG} = F_{IWG}^{Cl,WG}$.

$$\begin{aligned} & \left(U_1 \frac{1}{1 + H_{Cl}C_{Cl}} < \kappa_{Clwg} \quad \boxed{\text{or}} \quad U_1 \frac{H_{Cl}C_{Cl}}{1 + H_{Cl}C_{Cl}} > \kappa_{CNwg} \right) \quad \text{and} \quad F_{IWG1}^{Cl,WG} < \kappa_{WGwg} \\ & \left(U_2 \frac{1}{1 + H_{Cl}C_{Cl}} > \kappa_{Clwg} \quad \text{and} \quad U_2 \frac{H_{Cl}C_{Cl}}{1 + H_{Cl}C_{Cl}} < \kappa_{CNwg} \right) \quad \text{and} \quad F_{IWG2}^{Cl,WG} > \kappa_{WGwg} \\ & \quad \quad \quad (0 < \kappa_{Clwg} \quad \boxed{\text{or}} \quad 0 > \kappa_{CNwg}) \quad \text{and} \quad F_{IWG3}^{Cl,WG} < \kappa_{WGwg} \\ & \left(U_4 \frac{1}{1 + H_{Cl}C_{Cl}} < \kappa_{Clwg} \quad \boxed{\text{or}} \quad U_4 \frac{H_{Cl}C_{Cl}}{1 + H_{Cl}C_{Cl}} > \kappa_{CNwg} \right) \quad \text{and} \quad F_{IWG4}^{Cl,WG} < \kappa_{WGwg}. \end{aligned}$$

Case 2: only CI contributes to activation of wg . Here $wg_2^{WT} = \frac{\alpha_{Clwg}}{1 + \alpha_{Clwg}}$, so set $F_{IWG} = F_{IWG}^{Cl}$.

$$\begin{aligned} & \left(U_1 \frac{1}{1 + H_{Cl}C_{Cl}} < \kappa_{Clwg} \quad \boxed{\text{or}} \quad U_1 \frac{H_{Cl}C_{Cl}}{1 + H_{Cl}C_{Cl}} > \kappa_{CNwg} \right) \quad \text{and} \quad F_{IWG1}^{Cl} < \kappa_{WGwg} \\ & \left(U_2 \frac{1}{1 + H_{Cl}C_{Cl}} > \kappa_{Clwg} \quad \text{and} \quad U_2 \frac{H_{Cl}C_{Cl}}{1 + H_{Cl}C_{Cl}} < \kappa_{CNwg} \right) \quad \text{and} \quad F_{IWG2}^{Cl} < \kappa_{WGwg} \\ & \quad \quad \quad (0 < \kappa_{Clwg} \quad \boxed{\text{or}} \quad 0 > \kappa_{CNwg}) \quad \text{and} \quad F_{IWG3}^{Cl} < \kappa_{WGwg} \\ & \left(U_4 \frac{1}{1 + H_{Cl}C_{Cl}} < \kappa_{Clwg} \quad \boxed{\text{or}} \quad U_4 \frac{H_{Cl}C_{Cl}}{1 + H_{Cl}C_{Cl}} > \kappa_{CNwg} \right) \quad \text{and} \quad F_{IWG4}^{Cl} < \kappa_{WGwg}. \end{aligned}$$

Case 3: only IWG contributes to activation of wg . Here $wg_2^{WT} = \frac{\alpha_{WGwg}}{1+\alpha_{WGwg}}$, so set $F_{IWG} = F_{IWG}^{WG}$.

$$\begin{aligned} & \left(U_1 \frac{1}{1 + H_{Cl}C_{Cl}} < \kappa_{Clwg} \quad \boxed{\text{or}} \quad U_1 \frac{H_{Cl}C_{Cl}}{1 + H_{Cl}C_{Cl}} > \kappa_{CNwg} \right) \quad \text{and} \quad F_{IWG1}^{WG} < \kappa_{WGwg} \\ & \left(U_2 \frac{1}{1 + H_{Cl}C_{Cl}} < \kappa_{Clwg} \quad \boxed{\text{or}} \quad U_2 \frac{H_{Cl}C_{Cl}}{1 + H_{Cl}C_{Cl}} > \kappa_{CNwg} \right) \quad \text{and} \quad F_{IWG2}^{WG} > \kappa_{WGwg} \\ & \left(0 < \kappa_{Clwg} \quad \boxed{\text{or}} \quad 0 > \kappa_{CNwg} \right) \quad \text{and} \quad F_{IWG3}^{WG} < \kappa_{WGwg} \\ & \left(U_4 \frac{1}{1 + H_{Cl}C_{Cl}} < \kappa_{Clwg} \quad \boxed{\text{or}} \quad U_4 \frac{H_{Cl}C_{Cl}}{1 + H_{Cl}C_{Cl}} > \kappa_{CNwg} \right) \quad \text{and} \quad F_{IWG4}^{WG} < \kappa_{WGwg}. \end{aligned}$$

Note that a set of parameters that satisfies case 3 cannot satisfy any of the other two. This is because of the conditions on U_2 . For cases 1 and 2:

$$U_2 \frac{1}{1 + H_{Cl}C_{Cl}} > \kappa_{Clwg} \quad \text{and} \quad U_2 \frac{H_{Cl}C_{Cl}}{1 + H_{Cl}C_{Cl}} < \kappa_{CNwg},$$

while in case 3, the condition to be satisfied is exactly the negation of this. In other words, the region of parameter space defined by case 3 *cannot* be connected to regions defined by cases 1 and 2.

In addition, note that in cases 1 and 2, $U_2 = U_4$ leads to empty intervals for κ_{Clwg} , κ_{CNwg}). And a similarly conclusion holds when $U_2 = U_1$. This leads to four disconnected regions defined by: $U_1 > U_2 > U_4$, $U_2 > U_1, U_4$, $U_2 < U_1, U_4$ and $U_1 < U_2 < U_4$. It is now easy to check that, in each of these five regions, the intervals for the three parameters κ_{WGwg} , κ_{Clwg} , and κ_{CNwg} are as given in Table 8. ■

Table 6: Free parameters (physiological constraints, as in [3]).

Parameter	Interval
$U_{1,2,4}, T_2$	$(0, 1]$
T_1	$(0, T_2)$
$\alpha_{Clwg}, \alpha_{WGwg}$	$(0, 1)$
Half-lives (H_X)	$[5, 100]$
Transfer, cleavage ($C_{Cl}, r_{exo}, r_{endo}, r_M, r_{LM},$ $r_{LMPTC}, r_{MHH}, [HH]_0, [PTC]_0, \kappa_{PTCHH}$)	$(0, 1)$
$\kappa_{ENci}, \kappa_{ENhh}, \kappa_{CNhh}$	$(0, 1)$

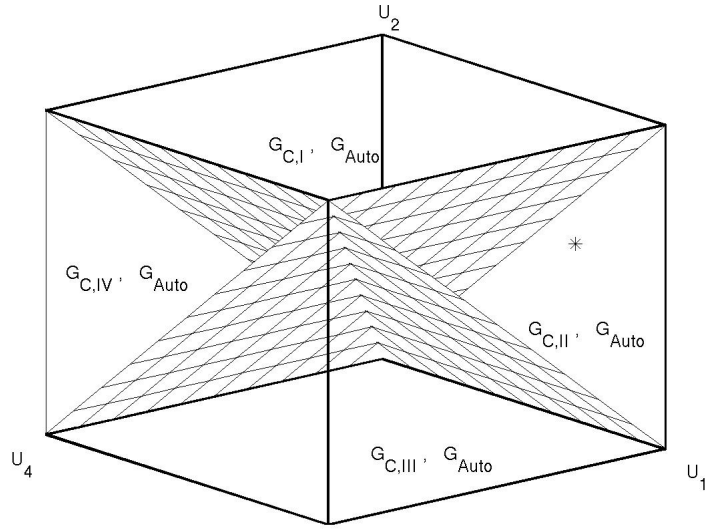


Figure 3: Projection of set G into the (U_1, U_2, U_4) space. The regions are defined by the planes $U_2 = U_4$ and $U_2 = U_1$. In region G_{Auto} , U_i can take values in the whole unitary cube, while $G_{C,I}$ through $G_{C,IV}$ do not include any of the points in the two planes. In this figure G_{Auto} appears to “intersect” all others, since they share values of U_i . However, this is only the projection effect, since not all parameters can be shown.

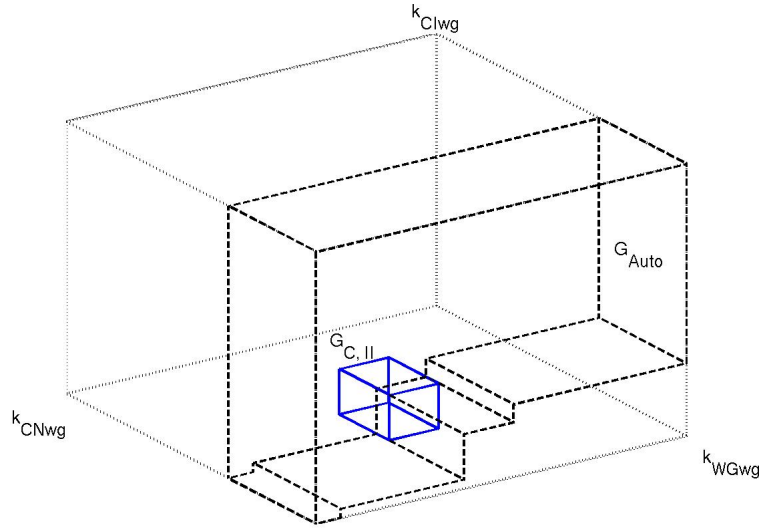


Figure 4: An example of regions $G_{C,II}$ (solid line rectangle) and G_{Auto} (dashed line polyhedron). This is the projection on the space $(k_{Clwg}, (k_{CNwg}, (k_{WGwg}))$, of the fibre over the point represented by “*” in Fig. 3. This point corresponds to choosing values for (U_1, U_2, U_4) in region $G_{C,II}$.

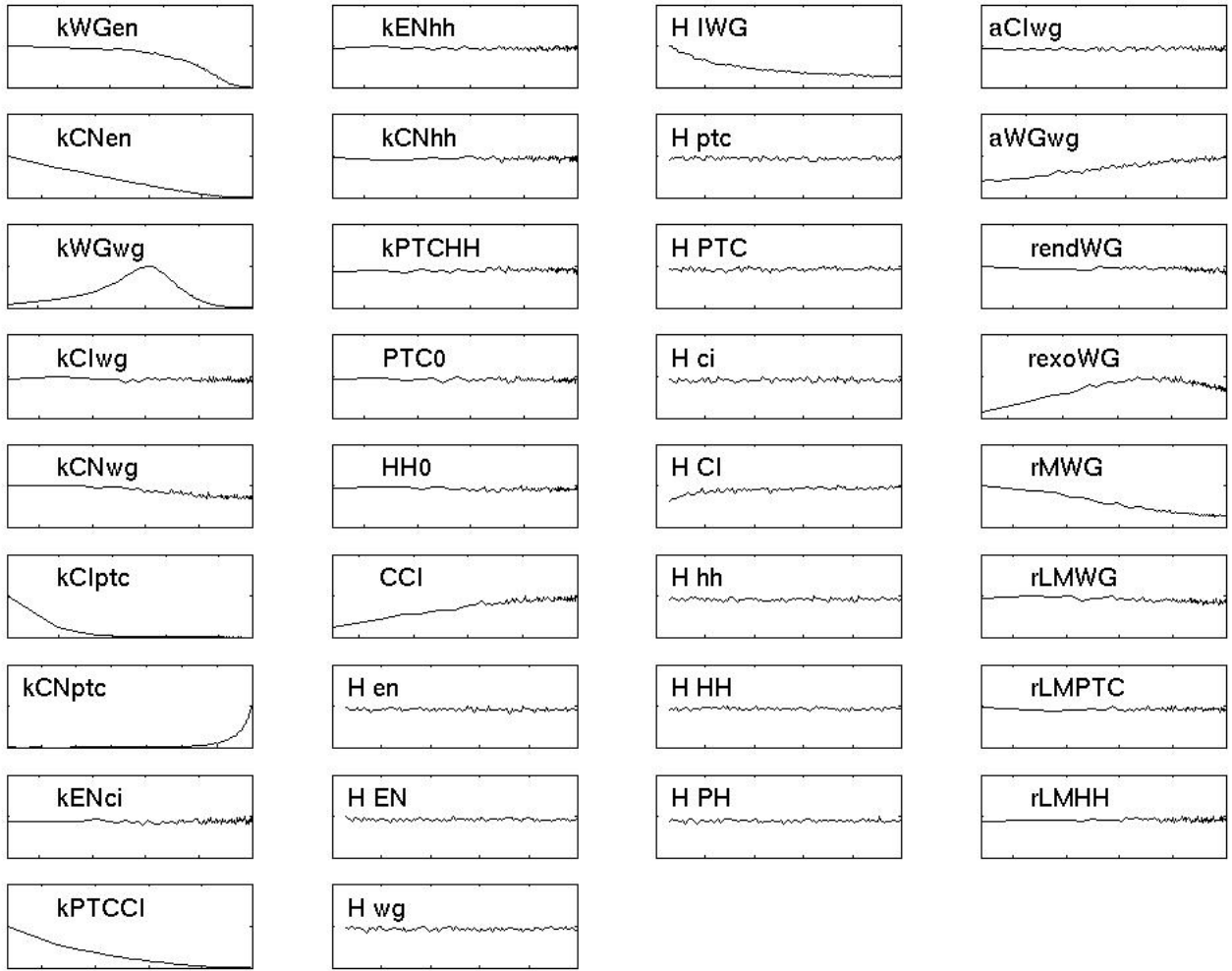


Figure 5: Parameter histograms out of 70026 parameter sets (refer to model equations for explanation of parameters). The notation and scales follow those of Fig. 6 in [13]. The half-lives (denoted H_x) range between 5 and 100 mins in a linear scale. The coefficients aCIwg and aWGwg range between 1.0 and 10.0 also in a linear scale. All other parameters range between 10^{-3} and 1, in \log_{10} scale.

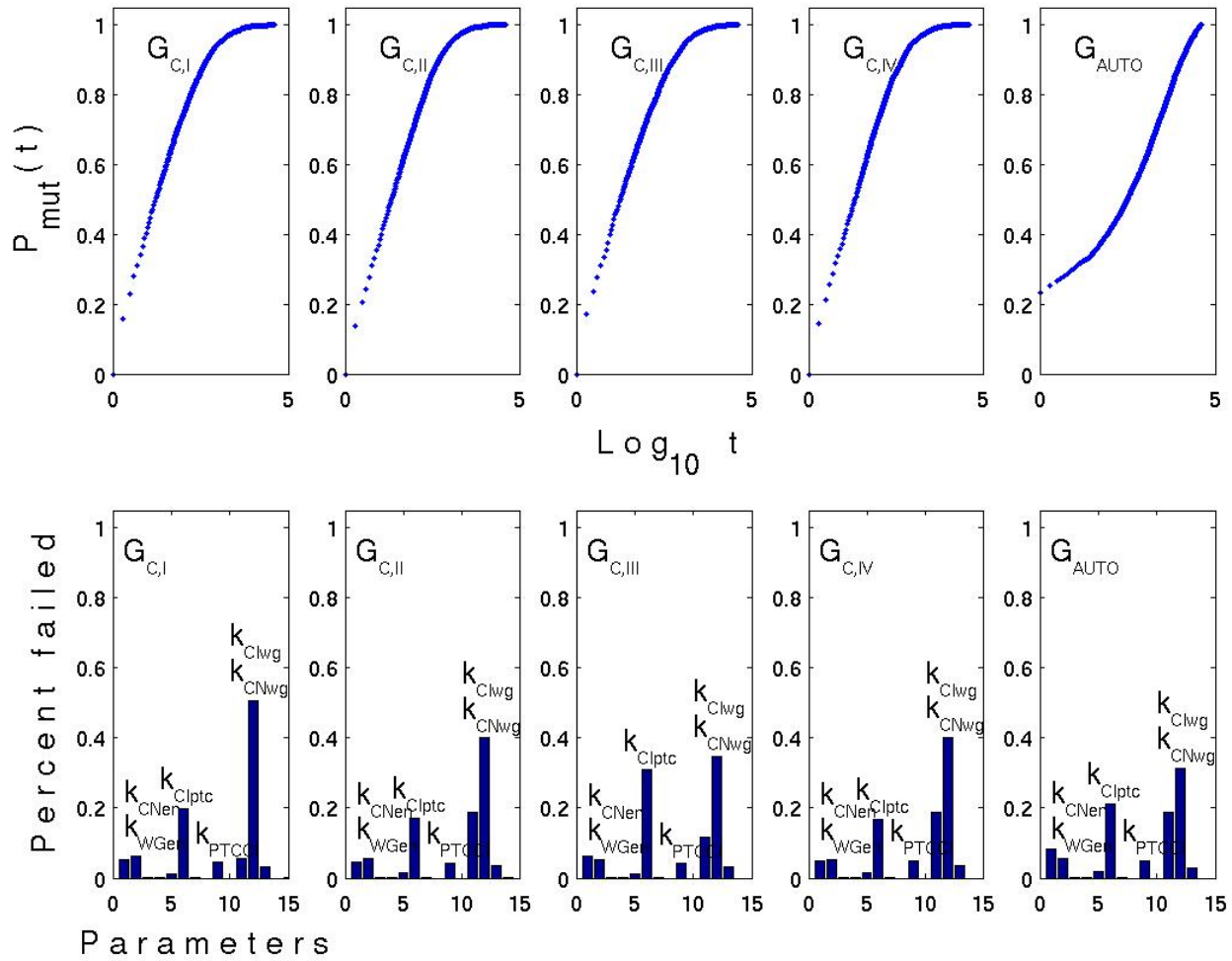


Figure 6: The distribution functions for the probability of leaving the region (or “mutation”), in each of the four regions. $P_{\text{mut}}(t)$ is shown in the top row, where the x axis is in logarithmic scale, and t ranges from 0 to 40000 (40000 is the maximal number of steps allowed in the random walks). The bottom row shows the failed parameters and the percentage of cases where each parameter failed (exit through a certain “face” of the polygonal regions).

Table 7: Parameters with constraints common to all regions.

Parameter	Interval
κ_{PTCCI}	$(0, \min\{T_1, F_{PTC2,T}\})$
κ_{Clptc}	$(0, \frac{1}{1+H_{Cl}C_{Cl}} \min\{U_1, U_2, U_4\})$
κ_{CNptc}	$(\frac{H_{Cl}C_{Cl}}{1+H_{Cl}C_{Cl}} \max\{U_1, U_2, U_4\}, 1)$
$\kappa_{CNen} \in (0, \frac{H_{Cl}C_{Cl}}{1+H_{Cl}C_{Cl}} \min\{U_1, U_2, U_4\})$ and $\kappa_{WGen} \in (0, F_{EWG3})$	
$\kappa_{CNen}, \kappa_{WGen}$	or
$\kappa_{CNen} \in (0, \frac{H_{Cl}C_{Cl}}{1+H_{Cl}C_{Cl}} \min\{U_1, U_2\})$ and $\kappa_{WGen} \in (F_{EWG4}, F_{EWG3})$	

Table 8: The five disconnected components.

Parameter	Interval	Region
κ_{Clwg}	$(\max\{U_1, U_4\} \frac{1}{1+H_{Cl}C_{Cl}}, U_2 \frac{1}{1+H_{Cl}C_{Cl}})$	$G_{C,I}$
κ_{CNwg}	$(U_2 \frac{H_{Cl}C_{Cl}}{1+H_{Cl}C_{Cl}}, 1)$	$U_2 > U_4, U_1$
κ_{Clwg}	$(U_4 \frac{1}{1+H_{Cl}C_{Cl}}, U_2 \frac{1}{1+H_{Cl}C_{Cl}})$	$G_{C,II}$
κ_{CNwg}	$(U_2 \frac{H_{Cl}C_{Cl}}{1+H_{Cl}C_{Cl}}, U_1 \frac{H_{Cl}C_{Cl}}{1+H_{Cl}C_{Cl}})$	$U_1 > U_2 > U_4$
κ_{Clwg}	$(0, U_2 \frac{1}{1+H_{Cl}C_{Cl}})$	$G_{C,III}$
κ_{CNwg}	$(U_2 \frac{H_{Cl}C_{Cl}}{1+H_{Cl}C_{Cl}}, \min\{U_1, U_4\} \frac{H_{Cl}C_{Cl}}{1+H_{Cl}C_{Cl}})$	$U_1, U_4 > U_2$
κ_{Clwg}	$(U_1 \frac{1}{1+H_{Cl}C_{Cl}}, U_2 \frac{1}{1+H_{Cl}C_{Cl}})$	$G_{C,IV}$
κ_{CNwg}	$(U_2 \frac{H_{Cl}C_{Cl}}{1+H_{Cl}C_{Cl}}, U_4 \frac{H_{Cl}C_{Cl}}{1+H_{Cl}C_{Cl}})$	$U_4 > U_2 > U_1$
$\kappa_{Clwg} \in (U_i \frac{1}{1+H_{Cl}C_{Cl}}, 1)$ or $\kappa_{CNwg} \in (0, U_i \frac{H_{Cl}C_{Cl}}{1+H_{Cl}C_{Cl}})$		G_{Auto}
$\kappa_{Clwg}, \kappa_{CNwg}$	for all $i = 1, 2, 4$	
κ_{Wwg}	$(\max\{F_{IWG1,2,3,4}^{Cl}, 1\})$ or $(\max\{F_{IWG1,3,4}^{Cl,WG}, F_{IWG2}^{Cl,WG}\})$	$G_{C,I}, G_{C,II}, G_{C,III}, G_{C,IV}$
κ_{Wwg}	$(\max\{F_{IWG1,3,4}^{WG}, F_{IWG2}^{WG}\})$	G_{Auto}